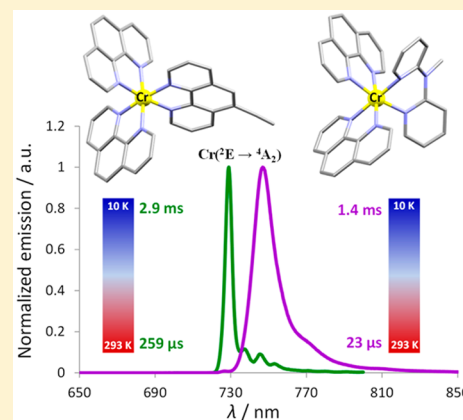


Heteroleptic Ter–Bidentate Cr(III) Complexes as Tunable Optical Sensitizers

Benjamin Doistau,^{*,†} Guillaume Collet,^{†,§} Emilio Acuña Bolomey,[†] Vida Sadat-Noorbakhsh,[†] Céline Besnard,[‡] and Claude Piguet^{*,†}[†]Department of Inorganic and Analytical Chemistry, University of Geneva, 30 quai Ernest Ansermet, CH-1211 Geneva 4, Switzerland[‡]Laboratory of Crystallography, University of Geneva, 24 quai Ernest Ansermet, CH-1211 Geneva 4, Switzerland

Supporting Information

ABSTRACT: To exploit Cr(III) coordination complexes as sensitizers in supramolecular energy-converting devices, the latter optical relays should display long-lived excited states, broad emission bands, and tunable spatial and electronic connections to activator units. An ad-hoc versatile strategy has been therefore developed for the preparation of a family of luminescent pseudo-octahedral $[\text{CrN}_6]$ chromophores made up of ter–bidentate heteroleptic $[\text{Cr}(\text{phen})_2(\text{N–N}')^{3+}]$ complexes, where phen is 1,10-phenanthroline, and N–N' stands for α,α' -diimine ligands possessing peripheral substituents compatible with both electronic tuning and structure extensions. As long as the ligand field in these $[\text{CrN}_6]$ chromophores remains sufficiently strong to avoid back-intersystem crossing, photophysical studies indicate that the lifetime of the near-infrared emissive $\text{Cr}^{(2)\text{E}}$ excited state is poorly sensitive to ligand-based electronic effects. On the contrary, a drop in symmetry, the coupling with high frequency oscillators, and the implementation of sterical constraints in heteroleptic $[\text{Cr}(\text{phen})_2(\text{N–N}')^{3+}]$ complexes affect both $\text{Cr}^{(2)\text{E}} \rightarrow {}^4\text{A}_2$ energies and $\text{Cr}^{(2)\text{E}}$ lifetimes. Altogether, $[\text{Cr}(\text{phen})_2(\text{phenAlkyn})]^{3+}$ (phenAlkyn = 5-ethynyl-1,10-phenanthroline) and $[\text{Cr}(\text{phen})_2(\text{dpma})]^{3+}$ (dpma = di(pyrid-2-yl)(methyl)amine) complexes mirror the favorable photophysical properties of homoleptic $[\text{Cr}(\text{phen})_3]^{3+}$ and thus emerge as the best heteroleptic candidates for acting as sensitizers at room temperature, and below 100 K, respectively, in more complicated architectures.



INTRODUCTION

Cr(III)-containing coordination complexes have recently attracted a renewal of interest for their magnetic, redox, and optical properties, which proved to be useful for various modern applications where this earth-abundant metal could advantageously replace rare ruthenium or platinum ores.^{1,2} First, the orbital-free magnetic moments of trivalent chromium complexes are ideally suited for rationalizing and optimizing (i) magnetic coupling,^{3–6} (ii) zero-field splitting,^{7–11} and (iii) single-molecular magnet behavior^{12,13} implemented in poly-metallic architectures.^{14–17} Second, the Cr(III) polypyridyl complexes are famous for displaying three successive ligand-centered¹¹ or one-metal-centered reductions,¹⁸ which allows their incorporation into memory devices.¹⁹ Third, the strongly oxidative $\text{Cr}^{(2)\text{E}}$ spin-flip excited state can be exploited (i) in photocathodic solar cells (by grafting chromium polypyridyl complexes onto semiconductor surfaces),²⁰ (ii) for carbon–carbon bond formation,^{21–23} and (iii) for water splitting and O_2 production.²⁴ Finally, the remarkable metal-centered optical properties of Cr(III) complexes associated with octahedral $[\text{CrO}_6]$ units found in solid oxides (weak ligand fields Δ and large Racah parameters B and C),^{25–29} which gave rise to the first ruby lasers, can be completely reversed in

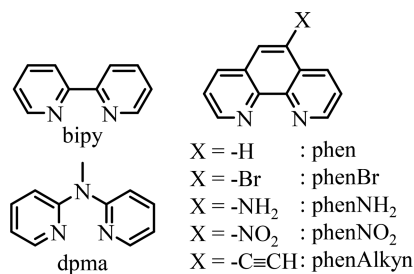
coordination complexes with the preparation of $[\text{CrN}_6]$ chromophores (strong ligand fields Δ and weak Racah parameters B and C)^{30–32} programmed for acting as sensitizers in molecular lanthanide-based energy transfer upconversion.^{33–36} The associated micro- to millisecond lifetimes (τ_S) observed for the metal-centered excited-state levels in $[\text{CrN}_6]$ complexes maximize energy transfer efficiency $\eta_{\text{ET}}^{\text{S} \rightarrow \text{A}}$ in sensitizer \rightarrow activator pair (eq 1)^{37,38} and are therefore well-adapted for being harnessed for the sensitization of nearby activators in polymetallic assemblies. ($k_S^{\text{rad}}\tau_S = \Phi_S$ corresponds to the intrinsic quantum yield of the donor emissive level. κ is the orientation factor between sensitizer and activator dipoles. n_r is the refractive index of the medium. N_{Av} is the Avogadro number in mol^{-1} .³⁸ r is the separation between donor and acceptor, and $J(\lambda)$ is the overlap integral between the emission spectrum of donor (S) and the absorption spectrum of the acceptor (A)).^{39–45}

Received: September 5, 2018

$$\eta_{\text{ET}}^{\text{S} \rightarrow \text{A}} = \frac{k_{\text{ET}}^{\text{S} \rightarrow \text{A}}}{k_{\text{ET}}^{\text{S} \rightarrow \text{A}} + k_{\text{S}}} = \left(1 + \frac{128\pi^5 n_{\text{r}}^4 N_{\text{Av}} r^6}{9(\ln 10) \kappa^2 J(\lambda) k_{\text{S}}^{\text{rad}} \tau_{\text{S}}} \right)^{-1} \quad (1)$$

Reasonably assuming comparable radiative rate constant ($k_{\text{S}}^{\text{rad}}$) for $[\text{CrN}_6]$ complexes with similar symmetries, the $\text{Cr}(\text{E})$ excited-state lifetime τ_{S} thus appears as the most relevant tunable parameter with $J(\lambda)$ and r for optimizing energy transfer efficiency ($\eta_{\text{ET}}^{\text{S} \rightarrow \text{A}}$). Despite these remarkable photo-physical properties, alternative $\text{Ru}(\text{II})$ chromophores, which display short $^3\text{MLCT}$ lifetimes within the microsecond range, are by far more exploited than $\text{Cr}(\text{III})$ as sensitizers in polymetallic devices; this is mainly because of the complicated and weakly developed synthetic strategies leading to heteroleptic chromium complexes.^{31,46,47,42} Currently limited to homoleptic complexes, $\text{Cr}(\text{III})$ -polypyridyl chromophores have been only sporadically involved as optical partners in polymetallic architectures^{48–51} exhibiting light downshifting⁵² or upconverted emission.^{33–36} Given that the well-known D_3 symmetrical ter-bidentate $[\text{Cr}(\text{bipy})_3]^{3+}$ or $[\text{Cr}(\text{phen})_3]^{3+}$ complexes (i) offer a large array of functionalization possibilities due to the rich bipy and phen ligand chemistry, (ii) display acceptable metal-centered lifetimes ($63 \mu\text{s} \leq \tau \leq 356 \mu\text{s}$), and (iii) may undergo specific ligand substitutions to give heteroleptic derivatives,^{30,39,42–44} the target $[\text{Cr}(\text{phen})_2(\text{N}-\text{N}')_2]^{3+}$ building blocks emerge as valuable and versatile candidates for working as heteroleptic sensitizers in extended polymetallic structures. However, the remarkable strategy developed by Kane-Maguire^{42,43} for the preparation of heteroleptic ter-bidentate chromium complexes does not tolerate electron-withdrawing ligands,^{42–44} and we are aware of a single recent report, in which this limitation was partially overcome via overheating under microwave radiation.¹⁹ To more globally solve this problem, we describe herein a novel versatile synthetic method that permits the synthesis of a complete family of heteroleptic $[\text{Cr}(\text{phen})_2(\text{N}-\text{N}')_2]^{3+}$ complexes with few, if any, electronic restrictions. This work then highlights how the variations in ligand-based electronic and geometrical characteristics (Scheme 1) affect the $\text{Cr}(\text{III})$

Scheme 1. Chemical Structures of the Bidentate Ligands Used in This Work



ligand-field and nephelauxetic parameters, together with their consequences on the degeneracy and lifetime of the emissive doublet excited state, two parameters which are crucial for further exploitation as sensitizers.

RESULTS AND DISCUSSIONS

Synthesis and Characterization of Heteroleptic Ter-Bidentate $\text{Cr}(\text{III})$ Complexes. The first step of the Kane-Maguire strategy^{42,53} was successfully reproduced in our hands

and gave the starting material $[\text{Cr}(\text{phen})_2\text{Cl}_2]\text{Cl}$ (**1**), the crystal structure of which was solved and is shown in Figure 1 (Figure S1 and Tables S1, S2, and S4 in the Supporting Information).⁵⁴

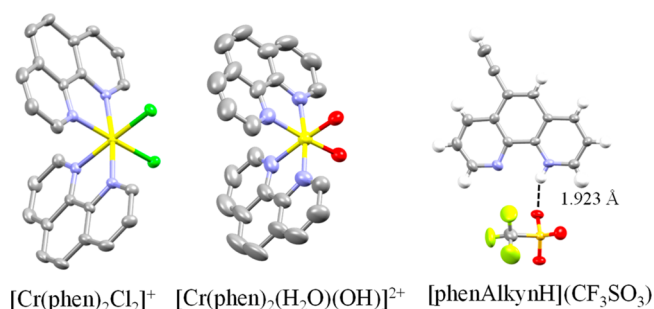


Figure 1. Molecular structures of the cations in the crystal structures of $[\text{Cr}(\text{phen})_2\text{Cl}_2]\text{Cl} \cdot (\text{CH}_3)_2\text{NCHO}$ (**1**), $[\text{Cr}(\text{phen})_2(\text{H}_2\text{O})(\text{OH})](\text{CF}_3\text{SO}_3)_2$ (**5**), and $[\text{phenAlkynH}](\text{CF}_3\text{SO}_3)$ (**4**) showing H bond length. Color code: Cr (yellow), C (gray), N (blue), O (red), S (orange), F (pale green), Cl (green). Ellipsoids are drawn at 50% probability. The Δ enantiomer is represented for each complex.

Subsequent reaction of $[\text{Cr}(\text{phen})_2\text{Cl}_2]\text{Cl}$ with trifluoromethanesulfonic acid, followed by precipitation in diethyl ether, led to the formation of the key intermediate $[\text{Cr}(\text{phen})_2(\text{CF}_3\text{SO}_3)_2]\text{CF}_3\text{SO}_3$. Addition of 1,10-phenanthroline (phen), or of 5-bromo-1,10-phenanthroline (phenBr), ultimately yielded, respectively, 41% and 66% of the target pure homoleptic $[\text{Cr}(\text{phen})_3](\text{PF}_6)_3$ (**2**, Figure 2; Figure S2 and Tables S1, S3, and S5)^{53,56} and heteroleptic $[\text{Cr}(\text{phen})_2(\text{phenBr})](\text{PF}_6)_3$ (**3**, Figure 2; Figure S5 and Tables S7, S8, and S10) complexes after metathesis with hexafluorophosphate anions. The latter synthetic method failed when using 1,10-phenanthroline possessing weak nitrogen donors as found in 5-nitro-phenanthroline (phenNO₂) or in a more delocalized π system as found in 5-ethynyl-1,10-phenanthroline (phenAlkyn). In the latter case, reaction of $[\text{Cr}(\text{phen})_2(\text{CF}_3\text{SO}_3)_2]\text{CF}_3\text{SO}_3$ with phenAlkyn resulted in the isolation of single crystals of off-white protonated ligand phenAlkynH (**4**, Figure 1; Figure S3 and Tables S6), together with $[\text{Cr}(\text{phen})_2(\text{H}_2\text{O})(\text{OH})](\text{CF}_3\text{SO}_3)_2$ complex (**5**, Figure 1, Figure S4 and Table S6) as red crystals, which suggest the competitive substitution of triflate anions with water molecules.

For the prevention of unwanted ligand protonation and complex hydrolysis, (i) $[\text{Cr}(\text{phen})_2\text{Cl}_2]\text{Cl}$ (**1**) was carefully dried under vacuum; (ii) $[\text{Cr}(\text{phen})_2(\text{CF}_3\text{SO}_3)_2]\text{CF}_3\text{SO}_3$ was immediately used after synthesis without storage, and last but not least, (iii) a sacrificial base was added during the last step for trapping the excess of trifluoromethanesulfonic acid. Pyridine, but especially sterically constrained 2,6-lutidine, was found to be well-suited for this purpose, since disastrous base-catalyzed $\text{Cr}(\text{III})$ complex hydrolysis could be avoided with these weak bases (Scheme 2).⁵⁷ It should be highlighted that tremendous ether washing of $[\text{Cr}(\text{phen})_2(\text{CF}_3\text{SO}_3)_2]\text{CF}_3\text{SO}_3$ intermediate under argon did not permit avoidance of the use of sacrificial base.

With this modified procedure in hand, $[\text{Cr}(\text{phen})_2(\text{phenAlkyn})](\text{BF}_4)_3$ (**6**, Figure 2; Figure S6 and Tables S7, S9, and S11), $[\text{Cr}(\text{phen})_2(\text{phenNO}_2)](\text{CF}_3\text{SO}_3)_3$ (**7**, Figure 2; Figure S7 and Tables S12, S13, and S15), $[\text{Cr}(\text{phen})_2(\text{phenNH}_2)](\text{CF}_3\text{SO}_3)_3$ (**8**, Figure 2; Figure S8

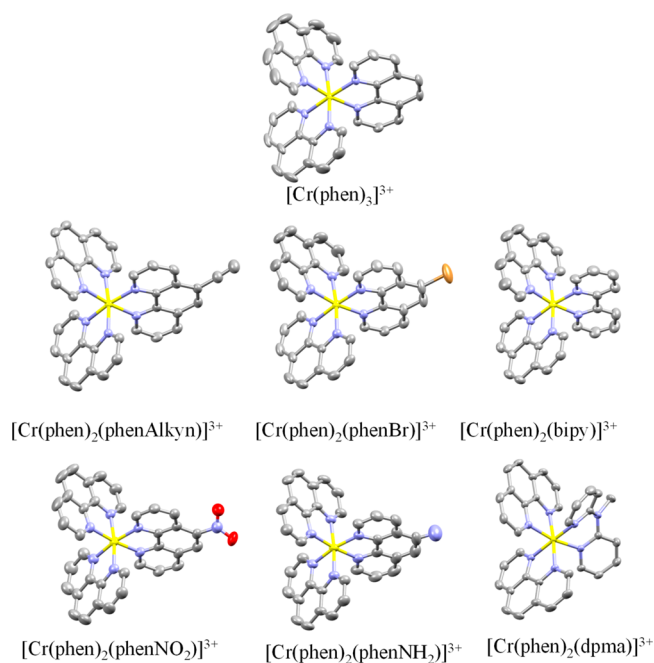


Figure 2. Molecular structures of the cationic complexes in the crystal structures of $[\text{Cr}(\text{phen})_3]_2(\text{PF}_6)_6 \cdot 6.33 \text{CH}_3\text{CN}$ (**2**), $[\text{Cr}(\text{phen})_2(\text{phenBr})](\text{PF}_6)_3 \cdot 2 \text{CH}_3\text{CN}$ (**3**), $[\text{Cr}(\text{phen})_2(\text{phenAlkyn})](\text{BF}_4)_3 \cdot 2 \text{CH}_3\text{CN}$ (**6**), $[\text{Cr}(\text{phen})_2(\text{phenNO}_2)](\text{CF}_3\text{SO}_3)_3$ (**7**), $[\text{Cr}(\text{phen})_2(\text{phenNH}_2)](\text{CF}_3\text{SO}_3)_3 \cdot 1.83 \text{CH}_3\text{CN}$ (**8**), $[\text{Cr}(\text{phen})_2(\text{bipy})](\text{CF}_3\text{SO}_3)_3$ (**9**) and $[\text{Cr}(\text{phen})_2(\text{dpma})](\text{CF}_3\text{SO}_3)_3$ (**10**). Cr (yellow), C (gray), N (blue), O (red), Br (brown). Ellipsoids are drawn at 50% probability. Hydrogens and counterions are omitted for clarity. The Δ enantiomer is represented for each complex.

and Tables S12, S14, and S16), $[\text{Cr}(\text{phen})_2(\text{bipy})](\text{CF}_3\text{SO}_3)_3$ (**9**, Figure 2; Figure S9 and Tables S17, S18, and S20), and $[\text{Cr}(\text{phen})_2(\text{dpma})](\text{CF}_3\text{SO}_3)_3$ (**10**, Figure 2; Figure S10 and Tables S17, S19, and S21) were obtained in good yields and without requiring large excess (maximum 2 equiv) of the entering N–N' ligands. All complexes were characterized by elemental analysis, ESI-MS, and X-ray-diffraction studies. In all cationic complexes, the three bidentate binding units are wrapped around a pseudo-3-fold axis passing through the chromium atom. Both Λ and Δ enantiomers are present in racemic proportion, which has no impact on the photophysical properties of the mononuclear heteroleptic complexes. However, it should be noted that further incorporation into polymetallic architectures might provide complicated mixtures of stereoisomers. Except for $[\text{Cr}(\text{phen})_2(\text{dpma})]^{3+}$ in **10**, in which the dpma ligand introduces an unusual six-membered chelate ring, all Cr–N bond lengths (2.045(4)–2.063(4) Å)

and chelate N–Cr–N bite angles (80.3(1)–81.1(1)°) are similar, whatever substituents are bound to the phenanthroline unit. Altogether, the $[\text{CrN}_6]$ chromophores can best be described as pseudo-octahedrons slightly compressed along the pseudo-3-fold helical axis (Table S22). As expected,^{32,18,58,59} the N–Cr–N bite angle in $[\text{Cr}(\text{phen})_2(\text{dpma})](\text{CF}_3\text{SO}_3)_3$ (**10**) is larger for dpma (85.4(1)°, six-membered chelate rings) than for phen ligand (80.0(1)°, five-membered chelate rings). The consequent increased overlap between the donor orbitals of dpma and 3d orbitals of trivalent chromium slightly shortens the Cr–N(dpma) distances (2.045(4) Å compared with 2.067(4) Å found for the partner phen ligands, Table S22). Neglecting for a while the specific peripheral substitution of the phenanthroline units, all the $[\text{CrN}_6]$ chromophores discussed above display local close-to- D_3 symmetry, except $[\text{Cr}(\text{phen})_2(\text{dpma})]^{3+}$, for which distortion from 3-fold symmetry becomes significant.

Photophysical Properties of Heteroleptic Ter–Bidentate Cr(III) Complexes: Ligand-Field Strength, Nephelauxetic Effect, and Symmetry. The key point here concerns the unusual large energy gap $\Delta E = \Delta - 9B - 3C + 50(B^2/\Delta)$ induced between the $\text{Cr}(^4\text{T}_2)$ and $\text{Cr}(^2\text{E})$ spectroscopic levels in pseudo-octahedral $[\text{CrN}_6]$ chromophore, which maximizes $\text{Cr}(^2\text{E} \rightarrow ^4\text{A}_2)$ phosphorescence and $\text{Cr}(^2\text{E})$ excited-state lifetimes via the reduced probability of phonon-assisted back-intersystem crossing (Figure 3).¹⁸

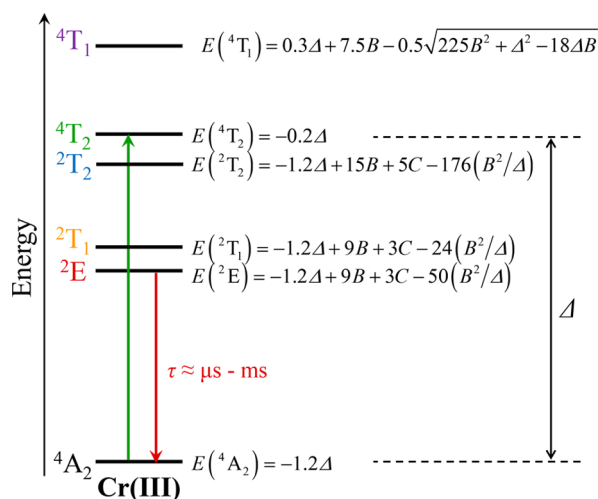
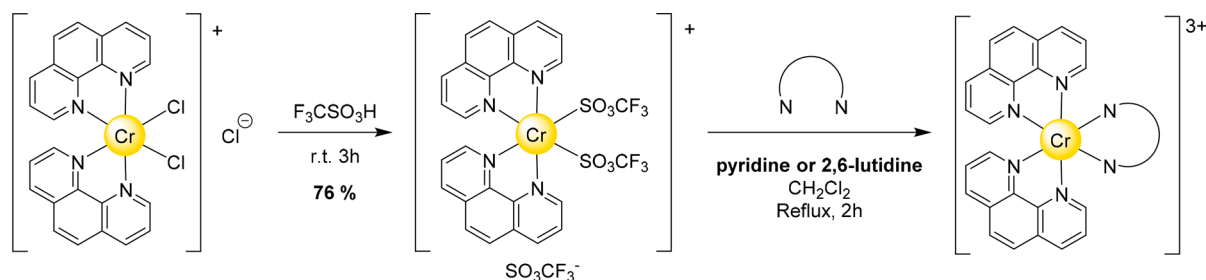


Figure 3. Energy level diagram for $[\text{Cr}(\text{III})\text{N}_6]$ chromophores in octahedral symmetry highlighting the lowest spin-allowed absorption (green arrow), and the lowest spin-forbidden emission (red arrow). The pertinent energy levels can be computed by using ligand field Δ , and Racah parameters B and C .^{60,61}

Scheme 2. Versatile Synthetic Strategy for the Preparation of Heteroleptic $[\text{Cr}(\text{phen})_2(\text{N}-\text{N}')^{3+}]$ Complexes



Among a large palette of homoleptic strong-field trivalent chromium complexes,^{27,62} $[\text{Cr}(\text{ddpd})_2]^{3+}$ was shown to display the longest room-temperature lifetime (898 μs , Figure 4 top),¹⁸ which can be further extended by 30% via systematic peripheral deuteration (1.2 ms).⁵⁸

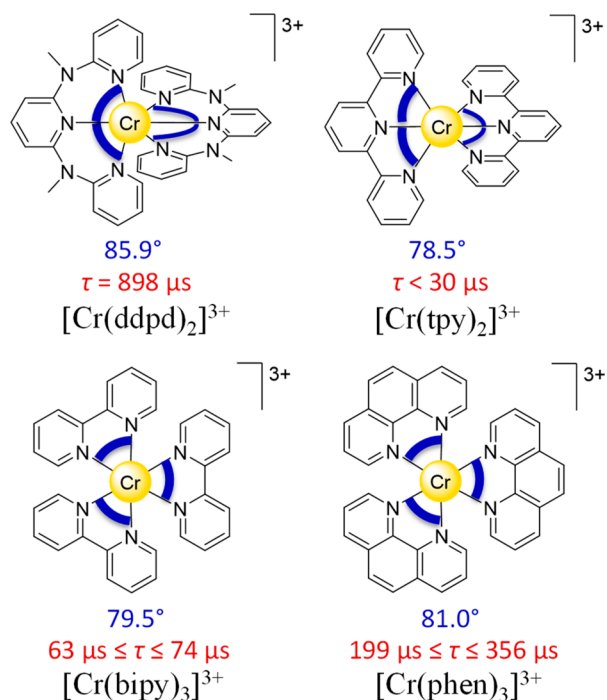


Figure 4. Chemical structures of homoleptic bis-terdentate (top) and ter-bidentate (bottom) chromium complexes where the average N–Cr–N chelate angles (blue), and emissive excited $\text{Cr}^{(2)}\text{E}$ lifetimes in solution at room temperature (red), are highlighted.^{31,18,64,65}

Those impressive features originate from (i) the weak energy of the $\text{Cr}^{(2)}\text{E}$ level ($12\,903\text{ cm}^{-1}$), combined with the strong ligand field induced by minor distortions from local octahedral symmetry which puts the $\text{Cr}^{(4)}\text{T}_2$ level at high energy ($22\,989\text{ cm}^{-1}$) and (ii) the promotion of $^2\text{E}/^4\text{A}_2$ surface crossing at high energy due to weak distortion from octahedra and anharmonic potential misalignment.^{63,32} The fused six-membered chelate rings produced by the ddpd ligand indeed fix average N–Cr–N chelate angles of 85.9° ,¹⁸ close to 90° compared with only 78.5° measured for fused five-membered chelate rings found in the analogous $[\text{Cr}(\text{tpy})_2]^{3+}$ complex (Figure 4 top).³¹ The associated short $\text{Cr}^{(2)}\text{E}$ lifetime measured for $[\text{Cr}(\text{tpy})_2]^{3+}$ ($\tau < 30\text{ }\mu\text{s}$) is however much less favorable for its use as an optical sensitizer. Moving toward ter-bidentate $[\text{Cr}(\text{bipy})_3]^{3+}$ or $[\text{Cr}(\text{phen})_3]^{3+}$ complexes (i) reduces the number of unfavorable constrained 5-membered chelate rings, thus restoring longer metal-centered lifetimes (Figure 4 bottom)^{64,65} and (ii) offers versatile access to $\text{Cr}(\text{III})$ complexes due to the rich chemistry of bipy or phen, compared to the weakly developed ddpd functionalization.

Room-temperature absorption spectra recorded for the CrN_6 complexes 2, 3, and 6–10 in the solid state and in acetonitrile solution (blue traces in Figure 5, Figures S11–S24) are dominated by weak spin-forbidden $\text{Cr}^{(2)}\text{E} \leftarrow ^4\text{A}_2$ and $\text{Cr}^{(2)}\text{T}_1 \leftarrow ^4\text{A}_2$ transitions at low energy ($13\,500\text{--}14\,500\text{ cm}^{-1}$, $\epsilon < 15\text{ L mol}^{-1}\text{ cm}^{-1}$), by moderately intense spin-allowed $\text{Cr}^{(4)}\text{T}_2 \leftarrow ^4\text{A}_2$ transitions at medium energy ($21\,000\text{--}22\,000\text{ cm}^{-1}$, $\epsilon \approx 50\text{--}500\text{ L mol}^{-1}\text{ cm}^{-1}$, the

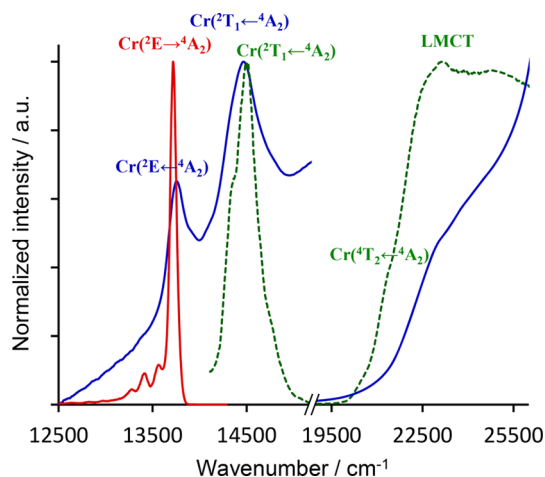


Figure 5. Normalized absorption spectra (full blue traces, solid state (left) and solution (right), 293 K), emission spectrum ($\lambda_{\text{exc}} = 355\text{ nm}$, $\bar{\nu}_{\text{exc}} = 28\,170\text{ cm}^{-1}$, red trace, frozen solution acetonitrile/propionitrile (6/4), 10 K) and excitation spectrum ($\lambda_{\text{em}} = 731\text{ nm}$ ($\bar{\nu}_{\text{em}} = 13\,680\text{ cm}^{-1}$), dashed green line, solid state, 10 K) recorded for $[\text{Cr}(\text{phen})_2(\text{phenAlkyn})](\text{BF}_4)_3$ (6). The spectroscopic labels are those pertinent to idealized octahedral symmetry.

spectroscopic labels assume O symmetry), by intense ligand-to-metal charge transfer (LMCT) and/or ligand-centered $^4[{}^3(\pi^* \leftarrow \pi)]$ transitions accompanied by spin-flip in the $^4\text{A}_2$ ground state ($22\,000\text{--}28\,000\text{ cm}^{-1}$, $\epsilon \approx 500\text{--}4000\text{ L mol}^{-1}\text{ cm}^{-1}$)^{66,45,67} and by ligand-centered $\pi^* \leftarrow \pi$ transitions at high energy ($>28\,000\text{ cm}^{-1}$; $\epsilon \approx 4000\text{--}20\,000\text{ L mol}^{-1}\text{ cm}^{-1}$, Table S23). It should be noted that an unambiguous discrimination between the $^4[{}^3(\pi^* \leftarrow \pi)]$ and $\text{Cr}^{(4)}\text{T}_2 \leftarrow ^4\text{A}_2$ transition is complicated, but (i) the lack of band structuration and (ii) their weak intensity ($\epsilon < 300\text{ L mol}^{-1}\text{ cm}^{-1}$) suggest assignment to ligand-field transitions.^{66,67} UV excitation into the ligand-centered absorption bands ($\lambda_{\text{exc}} = 355\text{ nm}$, $\bar{\nu}_{\text{exc}} = 28\,170\text{ cm}^{-1}$) provides low-temperature emission spectra with a single band (accompanied by vibrational progression at lower energy) assigned to the famous near-infrared spin-flip $\text{Cr}^{(2)}\text{E} \rightarrow ^4\text{A}_2$ luminescence (red trace in Figure 5, Figure S25 and Table S24). At room temperature, thermal equilibrium between the $^2\text{T}_1$ and ^2E states results in dual $\text{Cr}^{(2)}\text{T}_1 \rightarrow ^4\text{A}_2$ and $\text{Cr}^{(2)}\text{E} \rightarrow ^4\text{A}_2$ phosphorescence (Figure S26 and Table S25),⁶⁸ a phenomenon corroborated by excitation spectra recorded upon analyzing the $\text{Cr}^{(2)}\text{E} \rightarrow ^4\text{A}_2$ emissions, which demonstrate efficient sensitization originating from the close $\text{Cr}^{(2)}\text{T}_1$ level (green trace in Figure 5, Figures S27–S33 and Table S26). For all $[\text{CrN}_6]$ complexes displaying D_3 symmetry, the $\text{Cr}^{(2)}\text{T}_1 \leftarrow ^4\text{A}_2$ transition is split into two components (see the low-energy part of the green trace in Figure 5), which is diagnostic for a noticeable deviation from pure O symmetry in the $[\text{CrN}_6]$ chromophores. According to Endicott,⁶³ the drop in symmetry induced by the constrained chelate bite angles (transforming O_h into D_3 point groups, see previous section) results in the splitting of the t_{2g} orbitals (O_h symmetry) into $a_1 + e$ orbitals (D_3 symmetry) separated by a small energy gap. The interelectronic repulsions accompanying the filling of these orbitals with three electrons in $\text{Cr}(\text{III})$ complexes produce four spectroscopic levels: a $\text{Cr}^{(4)}\text{E}$ spin quartet ground state; a low-energy doubly degenerate doublet $\text{Cr}^{(2)}\text{E}$ excited level, reminiscent to that found in O symmetry; and two higher-energy doublet $\text{Cr}^{(2)}\text{A}_2 + \text{Cr}^{(2)}\text{E}$ levels, reminis-

cent to the $\text{Cr}({}^2\text{T}_1)$ level found in O symmetry. This explains the observation of three spin-flip absorption bands: two $\text{Cr}({}^2\text{E} \leftarrow {}^4\text{E})$ (arising from $\text{Cr}({}^2\text{T}_1 \leftarrow {}^4\text{A}_2)$ and $\text{Cr}({}^2\text{E} \leftarrow {}^4\text{A}_2)$ in O point group) and one $\text{Cr}({}^2\text{A}_2 \leftarrow {}^4\text{E})$ (arising from $\text{Cr}({}^2\text{T}_1 \leftarrow {}^4\text{A}_2)$ in O point group) for $[\text{CrN}_6]$ complexes in D_3 symmetry (Figure 5, low-energy blue trace).⁶³ Moreover, the energy gap between the half-occupied Cr-centered $a_1 + e$ orbitals produces some changes in the bonding parameters between the spin-flip excited states and the ground state.⁶³ The consequent shift in the nuclear coordinates is accompanied by minor, but non-negligible Stokes shifts ($\leq 38 \text{ cm}^{-1}$; 2 nm) together with vibronic progressions for the $\text{Cr}({}^2\text{E} \rightarrow {}^4\text{E})$ ($\text{Cr}({}^2\text{E} \rightarrow {}^4\text{A}_2)$ in O point group) emission bands as observed in $[\text{Cr}(\text{phen})_3](\text{PF}_6)_3$ (2), $[\text{Cr}(\text{phen})_2(\text{phenBr})](\text{PF}_6)_3$ (3), $[\text{Cr}(\text{phen})_2(\text{phenAlkyn})](\text{BF}_4)_3$ (6), $[\text{Cr}(\text{phen})_2(\text{phenNO}_2)](\text{CF}_3\text{SO}_3)_3$ (7), $[\text{Cr}(\text{phen})_2(\text{phenNH}_2)](\text{CF}_3\text{SO}_3)_3$ (8), and $[\text{Cr}(\text{phen})_2(\text{bipy})](\text{BF}_4)_3$ (9) (Figure 5 and Figures S11–S25). A detailed analysis of the vibronic progression, using anharmonic Morse potentials for modeling the energy gap $\Delta E = E(V+1) - E(V)$ between two adjacent vibrational levels of the ground state (ν_0 is the fundamental frequency and D the ground-state dissociation energy), is summarized in eq 2.⁶⁹

$$\Delta E = E(V+1) - E(V) = h\nu_0 - (V+1)\frac{(h\nu_0)^2}{2D} \quad (2)$$

Plots of $\Delta E = E(V+1) - E(V)$ as a function of $V+1$ indeed gave straight lines (Figure S34), from which $855 \leq D \leq 1920 \text{ cm}^{-1}$ and $163 \leq \nu_0/c \leq 182 \text{ cm}^{-1}$ can be calculated for the ground state (Table S27).⁶⁹ The vibronic progression induced by the release in symmetry involves Cr–N stretching modes ($163\text{--}182 \text{ cm}^{-1}$), which altogether spread the $\text{Cr}({}^2\text{E} \rightarrow {}^4\text{E})$ ($\text{Cr}({}^2\text{E} \rightarrow {}^4\text{A}_2)$ in O point group) emission band over 600 cm^{-1} . This represents a considerable advantage for maximizing the spectral overlap integrals $J(\lambda)$ between the Cr(III)-based sensitizer and nearby activators (eq 1). $[\text{Cr}(\text{phen})_2(\text{dpma})](\text{CF}_3\text{SO}_3)_3$ (10) undergoes a further drop in symmetry because the $[\text{CrN}_6]$ coordination sphere is now close to C_2 symmetry. Within this point group, only monodimensional irreducible representations are available, and the orbital degeneracies of the spin-flip $\text{Cr}({}^2\text{T}_1 \leftarrow {}^4\text{A}_2)$ and $\text{Cr}({}^2\text{E} \leftarrow {}^4\text{A}_2)$ transitions in O symmetry are completely lifted. We therefore expect and observe two groups of absorption in the NIR domain for $[\text{Cr}(\text{phen})_2(\text{dpma})]^{3+}$ with three (originating from the T term) and two (originating from the E term) components (Figure 6), respectively. The splitting of the $\text{Cr}({}^2\text{E})$ level is corroborated by the detection of dual NIR emission at 293 K (Figure S26). As a matter of clarity, throughout the rest of the study the O point group will be assumed for labeling energy levels.

As a consequence of the symmetry release, the global near-infrared emission of $[\text{Cr}(\text{phen})_2(\text{dpma})](\text{CF}_3\text{SO}_3)_3$ (10) is spread over 1300 cm^{-1} at 10 K, which makes this complex the most versatile candidate for optimizing spectral overlap between Cr(III) sensitizer and potential activators. The combination of the approximate equations gathered in Figure 3^{60,61} with the experimentally accessible energies found for the $\text{Cr}({}^4\text{T}_2)$, $\text{Cr}({}^2\text{T}_1)$, and $\text{Cr}({}^2\text{E})$ levels (relative to the $\text{Cr}({}^4\text{A}_2)$ ground state taken as a reference) provide (i) estimations for the ligand field Δ , and Racah parameters B and C (Table 1) together with (ii) predictions for the energies of the missing metal-centered energy levels $\text{Cr}({}^2\text{T}_2)$ and $\text{Cr}({}^4\text{T}_1)$ (Figure 7, these approximate calculations assume O point group).

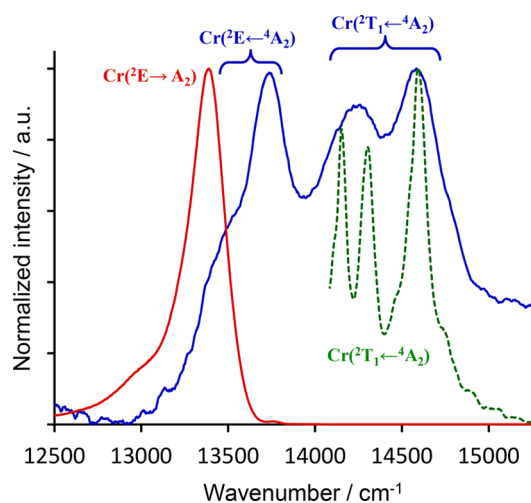


Figure 6. Normalized absorption spectrum (blue trace, solid state at 293 K), emission spectrum (red trace, frozen solution acetonitrile/propionitrile (6/4) at 10 K, $\lambda_{\text{exc}} = 355 \text{ nm}$, $\bar{\nu}_{\text{exc}} = 28\,169 \text{ cm}^{-1}$), and excitation spectrum (dashed green trace, solid state at 10 K, $\lambda_{\text{em}} = 747 \text{ nm}$, $\bar{\nu}_{\text{em}} = 13\,387 \text{ cm}^{-1}$) recorded for $[\text{Cr}(\text{phen})_2(\text{dpma})](\text{CF}_3\text{SO}_3)_3$ (10). The spectroscopic labels are those pertinent to idealized octahedral symmetry.

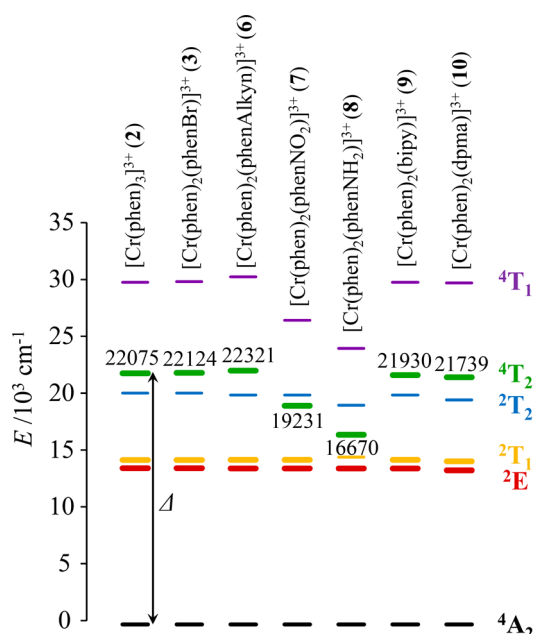
In absence of strong electron-withdrawing ($-\text{NO}_2$) or electron-donating ($-\text{NH}_2$) substituents, all heteroleptic $[\text{Cr}(\text{phen})_2(\text{N}-\text{N}')^{3+}]$ complexes display similar ligand fields ($\Delta \approx 22\,000 \text{ cm}^{-1}$, Figure 7) and nephelauxetic effects ($B \approx 800 \text{ cm}^{-1}$, Table 1) in agreement with the only minor structural variations found for these $[\text{CrN}_6]$ coordination units in their crystal structures. As expected, the strong inductive (Hammett coefficient $\sigma_I(\text{NO}_2) = 0.67$) and resonance (Hammett coefficient $\sigma_R(\text{NO}_2) = 0.16$) electron-withdrawing nitro group, when connected to one phenanthroline unit in $[\text{Cr}(\text{phen})_2(\text{phenNO}_2)](\text{CF}_3\text{SO}_3)_3$ (7), weakens the ligand field (Δ decreases) and reinforces the nephelauxetic effect (B decreases). As rather naive chemists, we originally expected that the connection of the opposite electron-donating amino group in $[\text{Cr}(\text{phen})_2(\text{phenNH}_2)](\text{CF}_3\text{SO}_3)_3$ (8) should result in the opposite trend. However, Hammett coefficients teach chemists that amino substituents, because of the presence of electronegative nitrogen atoms, are indeed (poor) σ -acceptors ($\sigma_I(\text{NH}_2) = 0.17$), while donation concerns only π effects ($\sigma_R(\text{NH}_2) = -0.48$).⁷⁰ With this in mind, some efficient π -overlap between filled phenNH_2 orbitals and $\text{Cr}(t_{2g})$ orbitals is expected to reduce Δ , while electron delocalization is simultaneously restricted to yield large Racah parameter B , a prediction in agreement with experimental data summarized in Figure 7. In addition to the detrimental N–H high-frequency multiphonon relaxation,^{71,28,72,73} the reduced $\text{Cr}({}^4\text{T}_2)$ – $\text{Cr}({}^2\text{E})$ energy gap in $[\text{Cr}(\text{phen})_2(\text{phenNH}_2)]^{3+}$ favors back-intersystem crossing (BISC), two characteristics which limit metal-centered phosphorescence as previously documented for analogous nonemissive bis-terpyridine Cr(III) complexes bearing an amino group.⁴⁵

Emissive Properties of Heteroleptic Ter–Bidentate Cr(III) Complexes: Excited-State Lifetimes. Time-resolved emissions demonstrate that the $\text{Cr}({}^2\text{E})$ emission lifetimes measured in heteroleptic $[\text{Cr}(\text{phen})_2(\text{N}-\text{N}')^{3+}]$ complexes strongly depend on temperature (Figure 8 and Tables S28 and S29). Beyond spontaneous radiative relaxation responsible for photon emission and modeled with the temperature-

Table 1. Ligand Fields Δ and Racah Parameters B and C for Pseudo-Octahedral $[\text{Cr}(\text{phen})_2(\text{N}-\text{N}')^{3+}]$ Complexes Deduced by Using the Equations Gathered in Figure 3 and the Experimental Cr-Centered ^2E , $^2\text{T}_1$, and $^4\text{T}_2$ Energies^a

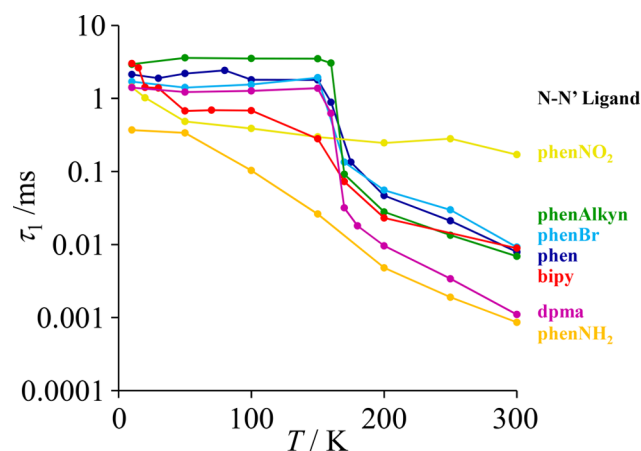
complex	$\sigma_{\text{N}-\text{N}'}^b$	$\sigma_{\text{R}}^{\text{N}-\text{N}'}^c$	Δ/cm^{-1}	B/cm^{-1}	C/cm^{-1}	Δ/B	C/B	E^d/cm^{-1}				
								^2E	$^2\text{T}_1$	$^4\text{T}_2$	$^2\text{T}_2^e$	$^4\text{T}_1^e$
$[\text{Cr}(\text{phen})_3]^{3+}$ (2)	0	0	22 075	779	2700	28	3.5	13 736	14 451	22 075	20 347	30 090
$[\text{Cr}(\text{phen})_2(\text{phenBr})]^{3+}$ (3)	0.47	−0.16	22 124	780	2697	28	3.5	13 736	14 451	22 124	20 347	30 150
$[\text{Cr}(\text{phen})_2(\text{phenAlkyn})]^{3+}$ (6)	0.29	0.08	22 321	805	2642	28	3.3	13 717	14 472	22 321	20 174	30 565
$[\text{Cr}(\text{phen})_2(\text{phenNO}_2)]^{3+}$ (7)	0.67	0.16	19 231	747	2815	26	3.8	13 717	14 472	19 231	20 174	26 754
$[\text{Cr}(\text{phen})_2(\text{phenNH}_2)]^{3+}$ (8) ^f	0.17	−0.48	16 670	803	2809	21	3.5 ^f	13 717	14 722 ^f	16 670	19 281	24 275
$[\text{Cr}(\text{phen})_2(\text{bipy})]^{3+}$ (9)			21 930	798	2663	27	3.3	13 717	14 472	21 930	20 174	30 085
$[\text{Cr}(\text{phen})_2(\text{dpma})]^{3+}$ (10)			21 739	816	2579	27	3.2	13 550	14 347	21 739	19 743	30 027

^aThe spectroscopic labels refer to pure O symmetry. For $[\text{Cr}(\text{phen})_2(\text{dpma})](\text{CF}_3\text{SO}_3)_3$ (10), the energies of parent $\text{Cr}(^2\text{T}_1)$ and $\text{Cr}(^2\text{E})$ levels were taken as the energy averages of their various components (see text). ^bHammett parameter estimating the inductive electronic effects of the substituent on the N–N' phenanthroline σ orbitals.⁷⁰ ^cHammett parameter estimating the resonance electronic effects of the substituent on the N–N' phenanthroline π orbitals.⁷⁰ ^dEnergies are given with respect to $\text{Cr}(^4\text{A}_2)$ ground state. ^eThe energies of $\text{Cr}(^2\text{T}_2)$ and $\text{Cr}(^4\text{T}_1)$ are computed. ^f $\text{Cr}(^2\text{T}_1 \leftarrow ^4\text{A}_2)$ was masked by LMCT bands. The ligand field Δ and Racah parameter B were determined assuming $C = 3.5B$.

**Figure 7.** Energy level diagram for $[\text{Cr}(\text{phen})_2(\text{N}-\text{N}')^{3+}]$ complexes, showing low-energy metal-centered levels (experimentally determined, thick trace; calculated, thin trace).

independent Einstein's law,^{74–76} competitive nonradiative $\text{Cr}(^2\text{E})$ depopulation can be induced by temperature-dependent phonon-assisted pathways such as (i) weak coupling with vibration modes that requires weak activation energy and persists at low temperature,²⁷ (ii) crossing with a photochemical intermediate in its ground electronic state (GSI),^{27,28} (iii) release of symmetry that induces anharmonic potential misalignment and the appearance of surface crossing between ^2E and $^4\text{A}_2$ states,^{28,63} (iv) surface crossing due to trigonal distortion in excited ^2E state induced by ligand steric strain relief,^{28,77} and (v) back-intersystem crossing (BISC) from ^2E to $^4\text{T}_2$ state.^{27,78} The latter mechanism is only significant for $^2\text{E}-^4\text{T}_2$ gap weaker than 3400 cm^{-1} as found in $[\text{CrN}_6]$ complexes.^{27,29,78,79}

The $\text{Cr}(^2\text{E})$ emission decays were measured in air-equilibrated acetonitrile/propionitrile (6/4) solution from 10 to 300 K (Figures S35–S45), and in degassed acetonitrile solution at 293 K (Figure S46) for the $[\text{Cr}(\text{phen})_2(\text{N}-\text{N}')^{3+}]$

**Figure 8.** Temperature-dependent $\text{Cr}(^2\text{E})$ emission lifetimes (τ_1), measured in a mixture of acetonitrile/propionitrile (6/4) ($5 \times 10^{-3}\text{ mol L}^{-1}$), of $[\text{Cr}(\text{phen})_3](\text{PF}_6)_3$ (2) (dark blue), $[\text{Cr}(\text{phen})_2(\text{phenBr})](\text{PF}_6)_3$ (3) (light blue), $[\text{Cr}(\text{phen})_2(\text{phenAlkyn})](\text{BF}_4)_3$ (6) (green), $[\text{Cr}(\text{phen})_2(\text{phenNO}_2)](\text{CF}_3\text{SO}_3)_3$ (7) (yellow, measured on powder samples since degradation occurred in propionitrile), $[\text{Cr}(\text{phen})_2(\text{phenNH}_2)](\text{CF}_3\text{SO}_3)_3$ (8) (orange), $[\text{Cr}(\text{phen})_2(\text{bipy})](\text{BF}_4)_3$ (9) (red), and $[\text{Cr}(\text{phen})_2(\text{dpma})](\text{CF}_3\text{SO}_3)_3$ (10) (purple).

complexes. From 10 to 150 K, the decay curves could be fitted with double exponential laws because of the formation of aggregates upon freezing, in which intermolecular energy transfers resulted in self-quenching and biexponential decays.^{80,38} Upon melting around 150 K, monoexponential decays were recovered in agreement with the existence of isolated solvated $\text{Cr}(\text{III})$ complexes. The double exponential fit observed in frozen solution can be thus partitioned between a short lifetime (τ_2), assigned to partially quenched $\text{Cr}(^2\text{E})$ levels found in aggregates, and a long lifetime (τ_1) assigned to $\text{Cr}(^2\text{E})$ levels in isolated complexes (Table S28). The $[\text{Cr}(\text{phen})_2(\text{phenNH}_2)]^{3+}$ complex systematically exhibits the shortest $\text{Cr}(^2\text{E})$ lifetimes of the series at any temperature (orange trace in Figure 8), because of the combined effect of (i) a reversible $\text{Cr}(^2\text{E}) \leftrightarrow \text{Cr}(^4\text{T}_2)$ back-intersystem crossing produced by the weak ligand field in this complex (Figure 7) since the energy gap $\Delta E(^2\text{E}-^4\text{T}_2) = 2950\text{ cm}^{-1}$ is below the upper limit of 3400 cm^{-1} set by Forster,^{27,78} and (ii) the presence of unfavorable high-energy N–H oscillators, which are famous for quenching the $\text{Cr}(^2\text{E})$ level.^{71,28,72,73} While

BISC is phonon-assisted and predominant at high temperature, the presence of N–H vibration modes opens a de-excitation pathway that requires weak thermal activation and persists at low temperature. All the other $[\text{Cr}(\text{phen})_2(\text{N}-\text{N}')^{3+}]$ complexes possess roughly constant $\text{Cr}^{(2)\text{E}}$ lifetimes in the millisecond range from 10 to 150 K in frozen solutions, which suggests the predominance of the radiative rate constant for the de-excitation of the $\text{Cr}^{(2)\text{E}}$ level at these temperatures. Upon melting around 150 K, an abrupt decrease of τ_1 results from the emergence of coupling processes with solvent vibrational modes and the operation of thermally activated relaxation processes. However, this abrupt decrease is not observed for $[\text{Cr}(\text{phen})_2(\text{phenNH}_2)]^{3+}$, probably because the deleterious effect of N–H vibration dominates the de-excitation processes and remains predominant upon solution melting regarding additional quenching processes produced by the diffusion of O_2 . At room temperature in oxygen-free acetonitrile, the decays of the $\text{Cr}^{(2)\text{E}}$ levels in $[\text{Cr}(\text{phen})_2(\text{N}-\text{N}')^{3+}]$ complexes are monoexponential (except $\text{N}-\text{N}' = \text{phenNH}_2$, Figure 9). They amount to about 200 μs , apart from $[\text{Cr}(\text{phen})_2(\text{phenNH}_2)]^{3+}$ and $[\text{Cr}(\text{phen})_2(\text{dpma})]^{3+}$ which show lifetime 2 orders of magnitude smaller than those found at 10 K (Table 2).

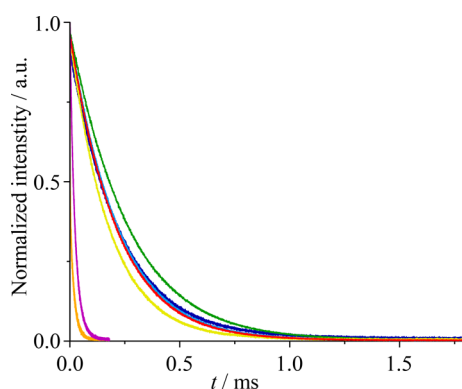


Figure 9. $\text{Cr}^{(2)\text{E}}$ emission decay curves measured in freeze-pump-thaw degassed acetonitrile (293 K, 10^{-4} mol L^{-1} , $\lambda_{\text{exc}} = 355$ nm) for $[\text{Cr}(\text{phen})_3](\text{PF}_6)_3$ (2, dark blue), $[\text{Cr}(\text{phen})_2(\text{phenBr})](\text{PF}_6)_3$ (3, light blue), $[\text{Cr}(\text{phen})_2(\text{phenAlkyn})](\text{BF}_4)_3$ (6, green), $[\text{Cr}(\text{phen})_2(\text{phenNO}_2)](\text{CF}_3\text{SO}_3)_3$ (7, yellow), $[\text{Cr}(\text{phen})_2(\text{phenNH}_2)](\text{CF}_3\text{SO}_3)_3$ (8, orange), $[\text{Cr}(\text{phen})_2(\text{bipy})](\text{BF}_4)_3$ (9, red), and $[\text{Cr}(\text{phen})_2(\text{dpma})](\text{CF}_3\text{SO}_3)_3$ (10, purple).

Close scrutiny at Figure 8 shows that $[\text{Cr}(\text{phen})_2(\text{bipy})](\text{BF}_4)_3$ (9) and $[\text{Cr}(\text{phen})_2(\text{dpma})](\text{CF}_3\text{SO}_3)_3$ (10) display maximum drops in lifetime in the 10–293 K range due to the additional rotational degrees of freedom found in bipy and dpma, compared with phen. This provides extra vibration modes for both complexes⁷² and larger anharmonic potential misalignment and surface crossing for $[\text{Cr}(\text{phen})_2(\text{dpma})]^{3+}$ justifying its particularly short lifetime (23 μs , Table 2) at 293 K in O_2 -free solution.^{63,77,28} Finally, $[\text{Cr}(\text{phen})_2(\text{phenAlkyn})](\text{BF}_4)_3$ (6) displays the longest lifetime in frozen solution below 150 K (around 3 ms), which remains non-negligible at room temperature in degassed solution (259 μs).

CONCLUSION

The use of noncoordinating and weakly basic 2,6-lutidine as a sacrificial base for trapping excess of acid extends the Kane-Maguire synthetic strategy to the preparation of kinetically

Table 2. $\text{Cr}^{(2)\text{E}}$ Emission Lifetimes (τ_1) for Heteroleptic $[\text{Cr}(\text{phen})_2(\text{N}-\text{N}')^{3+}]$ Complexes

complex	T/K	$\tau_1/\mu\text{s}$
$[\text{Cr}(\text{phen})_3](\text{PF}_6)_3$ (2)	10 ^a	2100
	293 ^b	224
$[\text{Cr}(\text{phen})_2(\text{phenBr})](\text{PF}_6)_3$ (3)	10 ^a	1700
	293 ^b	214
$[\text{Cr}(\text{phen})_2(\text{phenAlkyn})](\text{BF}_4)_3$ (6)	10 ^a	2900
	293 ^b	259
$[\text{Cr}(\text{phen})_2(\text{phenNO}_2)](\text{CF}_3\text{SO}_3)_3$ (7)	10 ^c	1400
	293 ^b	177
$[\text{Cr}(\text{phen})_2(\text{phenNH}_2)](\text{CF}_3\text{SO}_3)_3$ (8)	10 ^a	370
	293 ^b	17
$[\text{Cr}(\text{phen})_2(\text{bipy})](\text{BF}_4)_3$ (9)	10 ^a	3000
	208 ^b	208
$[\text{Cr}(\text{phen})_2(\text{dpma})](\text{CF}_3\text{SO}_3)_3$ (10)	10 ^a	1400
	293 ^b	23

^aLifetimes measured in air-equilibrated frozen acetonitrile/propionitrile (6/4) solutions ($C = 5 \times 10^{-3}$ mol L^{-1}). ^bLifetimes measured in freeze-pump-thaw degassed acetonitrile solution ($C = 10^{-4}$ mol L^{-1}). ^cLifetime measured in solid state.

inert heteroleptic ter-bidentate $\text{Cr}(\text{III})$ complexes $[\text{Cr}(\text{phen})_2(\text{N}-\text{N}')^{3+}]$, which may include electron-withdrawing or electron-donating bidentate ligands. Building on this success, both electronic properties and symmetry effects can be rationally implemented into $[\text{CrN}_6]$ chromophores for tuning their optical properties. First, pseudo- D_3 symmetry can be taken as a satisfying model for the analysis of both the coordination spheres (octahedrons compressed along the pseudo-3-fold axis) and the luminescence properties (two bands for the $\text{Cr}^{(2)\text{T}_1} \rightarrow {}^4\text{A}_2$) and one band for the $\text{Cr}^{(2)\text{E}} \rightarrow {}^4\text{A}_2$ spin-flip transitions derived from O symmetry) in $[\text{Cr}(\text{phen})_2(\text{N}-\text{N}')^{3+}]$. Second, the coexistence of five-membered and six-membered chelate rings in $[\text{Cr}(\text{phen})_2(\text{dpma})]^{3+}$ induces further deviation from trigonal symmetry, which significantly broadens the spectral domain covered by the NIR emission, an advantage for spectral overlap with low-energy acceptors obtained at the cost of additional nonradiative relaxation processes. Despite short room-temperature $\text{Cr}^{(2)\text{E}}$ lifetime, the combination of long $\text{Cr}^{(2)\text{E}}$ lifetime (1.4 ms) and large spectral width at 10 K makes $[\text{Cr}(\text{phen})_2(\text{dpma})]^{3+}$ compatible with sensitization in these specific conditions. With this in mind, $[\text{Cr}(\text{phen})_2(\text{phenAlkyn})]^{3+}$ finally emerges as the best and most versatile candidate for being selected as sensitizer in Cr-based optically active metallo-supramolecular assemblies. At 10 K, this complex possesses a long $\text{Cr}^{\text{III}}(^2\text{E})$ lifetime (2.9 ms) together with reasonably large spectral NIR emission (spread over 600 cm^{-1}). At room temperature, its excited-state lifetime in deoxygenated solution remains long enough (259 μs) for being exploited as relay, and the synthetic versatility of its $\text{C}\equiv\text{C}$ triple bond is compatible with its connections to neighboring activators.³¹

EXPERIMENTAL SECTION

General Procedures. ^1H and ^{13}C NMR spectra were recorded on a Bruker Avance 400 MHz spectrometer equipped with a variable-temperature unit. Chemical shifts were given in ppm with respect to tetramethylsilane $\text{Si}(\text{CH}_3)_4$. Pneumatically assisted electrospray (ESI) mass spectra were recorded from 10^{-4} M solutions on an Applied Biosystems API 150EX LC/MS system equipped with a Turbo Ionspray source. Elemental analyses were performed by K. L.

Buchwalder from the Microchemical Laboratory of the University of Geneva. Reagent-grade tetrahydrofuran and diethyl ether were distilled from sodium and benzophenone. Reagent-grade dichloromethane was distilled from CaH_2 . The 5-nitrophenanthroline (phenNO_2),⁸¹ 5-aminophenanthroline (phenNH_2),⁸¹ and di(pyrid-2-yl)(methyl)amine (dpma)⁸² were synthesized according to the literature procedures. All other chemicals were purchased from commercial sources and used without further purification. Silica-gel plates (Merck, 60 F₂₅₄) were used for thin-layer chromatography. Preparative column chromatography was performed using either neutral alumina gel from Fluka (Typ 507 C) 100–125 mesh or SiliaFlash silica gel P60 (0.04–0.063 mm).

Preparation of 5-Bromo-1,10-phenanthroline. A portion of 1,10-phenanthroline (7 g, 38.9 mmol, 1 equiv) was loaded in a heavy walled glass reaction tube equipped with a Teflon screw top fitted with a Viton O-ring. (See ref 83.) The vessel was put into an ice bath, and oleum (22–30%, 25 mL) and bromine (0.95 mL, 2.95 g, 18.4 mmol, 0.47 equiv) were added. The mixture was heated and stirred at 135 °C for 16 h. The solution was cooled to room temperature, poured into ice, and neutralized with KOH. The excess bromine was destroyed with sodium thiosulfate. The mixture was extracted three times with dichloromethane (3 × 200 mL). The combined organic phase was washed twice with water (2 × 300 mL), dried over MgSO_4 , filtered, and evaporated to dryness, providing 8.72 g of crude product. The solid was dissolved in minimum of dichloromethane, and then, Et_2O was added until the solution turned turbid. The flask was closed and the mixture left to crystallize overnight. The resulting solid was collected by filtration (5.51 g), and recrystallized using the same procedure to yield pure 5-bromo-1,10-phenanthroline (4.24 g, 42%).

¹H NMR (400 MHz, CDCl_3): δ 9.22 (m, 2H), 8.68 (dd, J = 8.4, 1.6 Hz, 1H), 8.20 (dd, J = 8.1, 1.8 Hz, 1H), 8.17 (s, 1H), 7.76 (dd, J = 8.4, 4.4 Hz, 1H), 7.66 (dd, J = 8.1, 4.3 Hz, 1H). ¹³C NMR (100 MHz, CDCl_3): δ 150.7, 150.5, 146.5, 145.5, 135.7, 134.9, 129.5, 128.6, 127.7, 123.6, 123.5, 120.6. ESI-MS m/z : $[\text{M} + \text{H}]^+$ ($\text{C}_{12}\text{H}_8\text{BrN}_2$): 259.3, 261.3.

Preparation of 5-Ethynyl-1,10-phenanthroline. Portions of 5-bromo-1,10-phenanthroline (4.0 g, 15.4 mmol, 1 equiv), $\text{PdCl}_2(\text{PPh}_3)_2$ (867 mg, 1.24 mmol, 8 mol %), CuI (472 mg, 2.48 mmol, 16 mol %), and a mixture of NEt_3 (28 mL)/THF (56 mL) previously degassed by argon bubbling (30 min) were introduced into a Schlenk tube under argon. Trimethylsilylacetylene (TMSA, 5.35 mL, 3.79 g, 38.5 mmol, 2.5 equiv) was then added. The mixture was stirred at 75 °C for 16 h. After solvent evaporation, the crude product was dissolved in dichloromethane (150 mL), and 4 mL of tris(2-aminoethyl)amine was added until the solution turned greenish blue. The organic layer was diluted to 500 mL, washed by water (4 × 300 mL), dried over anhydrous MgSO_4 , and filtered, and the solvent was evaporated. The resulting crude was purified by plug filtration (Al_2O_3 : $\text{CH}_2\text{Cl}_2/\text{MeOH}$ (0–3%)) providing 4.5 g of intermediate 5-[(trimethylsilyl)ethynyl]-1,10-phenanthroline. The latter compound was introduced into a round-bottom flask, dissolved in CH_2Cl_2 (50 mL), and completed with a solution of tetrabutylammonium fluoride (TBAF, 1 mol L^{−1} in THF, 21.2 mL, 21.2 mmol, 1.3 equiv). The mixture was stirred at room temperature for 15 min, and then diluted in CH_2Cl_2 (400 mL) and washed by water (4 × 300 mL) to afford 2.58 g of crude product. Purification by column chromatography (Al_2O_3 : $\text{CH}_2\text{Cl}_2/\text{acetone}$ (0–50%)), followed by trituration and stirring of the final solid during 2 h in Et_2O (25 mL), yielded pure 5-ethynyl-1,10-phenanthroline (1.428 g, 7.0 mmol, 45%) as an off-white solid. ¹H NMR (400 MHz, CDCl_3): δ 9.23 (dd, J = 4.3, 1.7 Hz, 1H), 9.21 (dd, J = 4.4, 1.7 Hz, 1H), 8.77 (dd, J = 8.2, 1.7 Hz, 1H), 8.23 (dd, J = 8.1, 1.7 Hz, 1H), 8.09 (s, 1H), 7.73 (dd, J = 8.3, 4.3 Hz, 1H), 7.66 (dd, J = 8.1, 4.4 Hz, 1H), 3.55 (s, 1H). ¹³C NMR (100 MHz, CDCl_3): δ 151.3, 150.9, 146.5, 146.0, 136.0, 134.7, 131.9, 128.4, 127.9, 123.6, 123.5, 119.0, 83.3, 80.2. ESI-MS m/z : $[\text{M} + \text{H}]^+$ ($\text{C}_{14}\text{H}_9\text{N}_2$), 204.4; $[2\text{M} + \text{H}]^+$ ($\text{C}_{28}\text{H}_{17}\text{N}_4$), 409.1.

Preparation of $[\text{Cr}(\text{phen})_2\text{Cl}_2]\text{Cl}$ (1). CrCl_3 anhydrous (0.56 g, 3.55 mmol, 1 equiv), 1,10-phenanthroline (2.00 g, 11.13 mmol, 3.1 equiv), and absolute ethanol (20 mL) were introduced into a round-bottom flask. (See ref 84.) The mixture was heated to reflux, and three

tablets of zinc (1.2 g) were added. The mixture was heated to reflux during 10 min. The produced green solid was filtered over a PTFE membrane and dried with Et_2O . Removal of excess of Zn tabs with tweezers afforded 93% (1.71 g) of $[\text{Cr}(\text{phen})_2\text{Cl}_2]\text{Cl}$ as a green powder. Elemental Anal. Calcd (%) for $[\text{Cr}(\text{phen})_2\text{Cl}_2]\text{Cl} \cdot 1.2\text{H}_2\text{O} \cdot 1.5\text{EtOH}$: C, 53.21; H, 4.53; N, 9.19. Found: C, 53.26; H, 4.33; N, 9.00. Slow diffusion of Et_2O into a solution of $[\text{Cr}(\text{phen})_2\text{Cl}_2]\text{Cl}$ in DMF provided green single crystals suitable for XRD.

Preparation of $[\text{Cr}(\text{phen})_2(\text{CF}_3\text{SO}_3)_2](\text{CF}_3\text{SO}_3)$. Trifluoromethanesulfonic acid (7 mL) was added to $[\text{Cr}(\text{phen})_2\text{Cl}_2]\text{Cl}$ (1.5 g, 2.89 mmol) into a Schlenk tube under argon and heated at 100 °C for 2 h with argon bubbling. (See refs 30, 42, and 53.) The solution was cooled on ice and vigorously stirred. Anhydrous distilled diethyl ether (40 mL) was added and led to the formation of a pink precipitate. The solid was filtered under argon, washed twice with anhydrous diethyl ether, and transferred into the glovebox where the pink precipitate was stored $[\text{Cr}(\text{phen})_2(\text{CF}_3\text{SO}_3)_2](\text{CF}_3\text{SO}_3)$ (2.51 g, 2.49 mmol, yield 86%). ESI-MS m/z : $[\text{Cr}(\text{phen})_2(\text{CF}_3\text{SO}_3)_2]^+$, 710.4. Elemental Anal. Calcd (%) for $[\text{Cr}(\text{phen})_2(\text{CF}_3\text{SO}_3)_2](\text{CF}_3\text{SO}_3) \cdot 1.1\text{HSO}_3\text{CF}_3$: C, 32.94; H, 1.68; N, 5.47. Found: C, 33.22; H, 1.85; N, 5.25.

Preparation of $[\text{Cr}(\text{phen})_3](\text{PF}_6)_3$ (2). $[\text{Cr}(\text{phen})_2(\text{CF}_3\text{SO}_3)_2](\text{CF}_3\text{SO}_3)$ (200 mg, 0.232 mmol, 1 equiv), 1,10-phenanthroline (126 mg, 0.636 mmol, 2.7 equiv), and anhydrous distilled dichloromethane (15 mL) were introduced into a Schlenk tube under argon. The reaction mixture was heated at 45 °C for 90 min. The resulting yellow solid was filtered on a PTFE membrane, washed with CH_2Cl_2 , and dried with diethyl ether to give pure $[\text{Cr}(\text{phen})_3](\text{CF}_3\text{SO}_3)_3$ (98 mg, 0.094 mmol, yield 41%). Metathesis resulted from the dissolution of $[\text{Cr}(\text{phen})_3](\text{CF}_3\text{SO}_3)_3$ in a minimum amount of MeOH, followed by the addition of a saturated solution of TBAPF₆ in MeOH. The resulting precipitate of $[\text{Cr}(\text{phen})_3](\text{PF}_6)_3$ was filtered and dried. Slow diffusion of Et_2O into a solution of $[\text{Cr}(\text{phen})_3](\text{PF}_6)_3$ in acetonitrile provided single crystals suitable for XRD. ESI-MS m/z : $[[\text{Cr}(\text{phen})_3](\text{CF}_3\text{SO}_3)_2]^+$, 890.7. Elemental Anal. Calcd (%) for $[\text{Cr}(\text{phen})_3](\text{CF}_3\text{SO}_3)_3 \cdot 1.2\text{H}_2\text{O}$: C, 43.13; H, 2.51; N, 7.92. Found: C, 44.05; H, 2.39; N, 7.85. Elemental Anal. Calcd (%) for $[\text{Cr}(\text{phen})_3](\text{PF}_6)_3$: C, 42.08; H, 2.35; N, 8.18. Found: C, 42.25; H, 2.38; N, 8.10.

Preparation of $[\text{Cr}(\text{phen})_2(\text{phenBr})](\text{PF}_6)_3$ (3). $[\text{Cr}(\text{phen})_2(\text{CF}_3\text{SO}_3)_2](\text{CF}_3\text{SO}_3)$ (51 mg, 0.06 mmol), 5-bromo-1,10-phenanthroline (38 mg, 0.15 mmol), and anhydrous distilled dichloromethane (7 mL) were introduced into a Schlenk tube. The reaction mixture was heated at 45 °C for 3 h. The formed yellow solid was filtered on a PTFE membrane, washed with CH_2Cl_2 , and dried with Et_2O to give pure $[\text{Cr}(\text{phen})_2(\text{phenBr})](\text{CF}_3\text{SO}_3)_3$ (44 mg, 0.04 mmol, yield 66%). Metathesis resulted from the dissolution of $[\text{Cr}(\text{phen})_2(\text{phenBr})](\text{CF}_3\text{SO}_3)_3$ in a minimum amount of MeOH, followed by the addition of a saturated solution of TBAPF₆ in MeOH. The precipitate of $[\text{Cr}(\text{phen})_2(\text{phenBr})](\text{PF}_6)_3$ was filtered and dried. Slow diffusion of Et_2O into a solution of $[\text{Cr}(\text{phen})_2(\text{phenBr})](\text{PF}_6)_3$ in acetonitrile provided single crystals suitable for XRD. ESI-MS m/z : $[[\text{Cr}(\text{phen})_2(\text{phenBr})](\text{CF}_3\text{SO}_3)_2]^+$, 970.6. Elemental Anal. Calcd (%) for $[\text{Cr}(\text{phen})_2(\text{phenBr})](\text{CF}_3\text{SO}_3)_3 \cdot 2\text{H}_2\text{O}$: C, 40.57; H, 2.36; N, 7.28. Found: C, 40.48; H, 2.51; N, 7.14.

General Preparation of $[\text{Cr}(\text{phen})_2(\text{N}-\text{N}')](\text{CF}_3\text{SO}_3)_3$ Complexes. $[\text{Cr}(\text{phen})_2\text{Cl}_2]\text{Cl}$ (1 equiv) and trifluoromethanesulfonic acid (1 mL per 120 mg of $[\text{Cr}(\text{phen})_2\text{Cl}_2]\text{Cl}$) were introduced into a Schlenk tube under argon and heated at 100 °C for 2 h with argon bubbling. The solution was cooled on ice and vigorously stirred. Anhydrous distilled diethyl ether (10 mL per 200–300 mg of $[\text{Cr}(\text{phen})_2\text{Cl}_2]\text{Cl}$) was added, thus leading to the formation of a pink precipitate. The solid was filtered under argon, washed twice with anhydrous diethyl ether, rapidly dissolved in distilled CH_2Cl_2 (10 mL), and transferred under argon into a Schlenk tube containing the N–N' ligand, pyridine or 2,6-lutidine, and distilled CH_2Cl_2 (10 mL). The resulting mixture was stirred at 45 °C during 2–16 h until formation of a large amount of precipitate. The solid was collected by filtration on a PTFE membrane, washed with CH_2Cl_2 , and dried with

Et₂O to give [Cr(phen)₂(N–N')](CF₃SO₃)₃ complexes as a microcrystalline solid.

Preparation of [Cr(phen)₂(phenAlkyn)](BF₄)₃ (6). This complex was synthesized according to the general synthetic method described for [Cr(phen)₂(N–N')](CF₃SO₃)₃ complexes.

[Cr(phen)₂Cl₂]Cl (200 mg, 0.387 mmol, 1 equiv), trifluoromethanesulfonic acid (2 mL), 5-ethynyl-1,10-phenanthroline (79 mg, 0.387 mmol, 1 equiv), and pyridine (62 μL, 0.774 mmol, 2 equiv) were reacted with a reaction time of 2 h.

This method afforded pure [Cr(phen)₂(phenAlkyn)](CF₃SO₃)₃ (300 mg, 73%). Metathesis resulted from the dissolution of [Cr(phen)₂(phenAlkyn)](CF₃SO₃)₃ in a minimum amount of MeOH, followed by the addition of a saturated solution of TBABF₄ in MeOH. The precipitate of [Cr(phen)₂(phenAlkyn)](BF₄)₃ was filtered and dried. Slow diffusion of Et₂O into a solution of [Cr(phen)₂(phenAlkyn)](BF₄)₃ in acetonitrile provided single crystals suitable for XRD. ESI-MS *m/z*: [[Cr(phen)₂(phenAlkyn)](CF₃SO₃)₂]⁺, 914.5. Elemental Anal. Calcd (%) for [Cr(phen)₂(phenAlkyn)](CF₃SO₃)₃·2.5H₂O: C, 44.41; H, 2.64; N, 7.58. Found: C, 44.37; H, 2.53; N, 7.63. Elemental Anal. Calcd (%) for [Cr(phen)₂(phenAlkyn)](BF₄)₃·1.2H₂O: C, 50.91; H, 2.96; N, 9.35. Found: C, 50.91; H, 3.00; N, 9.23.

Preparation of [Cr(phen)₂(phenNO₂)](CF₃SO₃)₃ (7). The complex was synthesized according to the general synthetic method described for [Cr(phen)₂(N–N')](CF₃SO₃)₃ complexes.

[Cr(phen)₂Cl₂]Cl (200 mg, 0.387 mmol, 1 equiv), trifluoromethanesulfonic acid (2 mL), 5-nitro-1,10-phenanthroline (176 mg, 0.772 mmol, 2 equiv), and 2,6-lutidine (45 μL, 0.386 mmol, 1 equiv) were reacted with a reaction time of 16 h. The resulting yellow powder was suspended in CH₂Cl₂, stirred thoroughly for 24 h, filtered on a PTFE membrane, washed with CH₂Cl₂, and dried with Et₂O to give pure [Cr(phen)₂(phenNO₂)](CF₃SO₃)₃ (186 mg, yield 44%). Slow diffusion of Et₂O in a solution of [Cr(phen)₂(phenNO₂)](CF₃SO₃)₃ in methanol provided single crystals suitable for XRD. ESI-MS *m/z*: [[Cr(phen)₂(phenNO₂)](CF₃SO₃)₂]⁺, 935.5. Elemental Anal. Calcd (%) for [Cr(phen)₂(phenNO₂)](CF₃SO₃)₃·2.5H₂O: C, 41.46; H, 2.50; N, 8.68. Found: C, 41.41; H, 2.38; N, 8.63.

Preparation of [Cr(phen)₂(phenNH₂)](CF₃SO₃)₃ (8). The complex was synthesized according to the general synthetic method described for [Cr(phen)₂(N–N')](CF₃SO₃)₃ complexes.

[Cr(phen)₂Cl₂]Cl (200 mg, 0.387 mmol, 1 equiv), trifluoromethanesulfonic acid (2 mL), 5-amino-1,10-phenanthroline (90 mg, 0.463 mmol, 1.2 equiv), and pyridine (50 μL, 0.521 mmol, 1.35 equiv) were reacted with a reaction time of 16 h. The resulting brown powder was thoroughly washed with THF, filtered on a PTFE membrane, washed with CH₂Cl₂, and dried with Et₂O to give pure [Cr(phen)₂(phenNH₂)](CF₃SO₃)₃ (260 mg, yield 64%). Slow diffusion of Et₂O into a solution of [Cr(phen)₂(phenNH₂)](CF₃SO₃)₃ in acetonitrile provided single crystals suitable for XRD. ESI-MS *m/z*: [[Cr(phen)₂(phenNH₂)](CF₃SO₃)₂]⁺, 905.5. Elemental Anal. Calcd (%) for [Cr(phen)₂(phenNH₂)](CF₃SO₃)₃·1.5H₂O: C, 43.30; H, 2.61; N, 9.06. Found: C, 43.40; H, 2.70; N, 8.96.

Preparation of [Cr(phen)₂(bipy)](BF₄)₃ (9). The complex was synthesized according to the general synthetic method described for [Cr(phen)₂(N–N')](CF₃SO₃)₃ complexes.

[Cr(phen)₂Cl₂]Cl (300 mg, 0.578 mmol, 1 equiv), trifluoromethanesulfonic acid (2.2 mL), bipyridine (181 mg, 1.16 mmol, 2 equiv), and pyridine (93 μL, 1.16 mmol, 2 equiv) were reacted with a reaction time of 2 h. This method afforded pure [Cr(phen)₂(bipy)](CF₃SO₃)₃ (444 mg, yield 76%). Metathesis resulted from the dissolution of [Cr(phen)₂(bipy)](CF₃SO₃)₃ in a minimum amount of MeOH, followed by the addition of a saturated solution of TBABF₄ in MeOH. The precipitate of [Cr(phen)₂(bipy)](BF₄)₃ was filtered and dried. Slow diffusion of Et₂O into a solution of [Cr(phen)₂(bipy)](CF₃SO₃)₃ in acetonitrile provided single crystals suitable for XRD. ESI-MS *m/z*: [[Cr(phen)₂(bipy)](CF₃SO₃)₂]⁺, 866.5. Elemental Anal. Calcd (%) for [Cr(phen)₂(bipy)](CF₃SO₃)₃·1.3CH₂Cl₂: C, 40.85; H, 2.38; N, 7.46. Found: C, 40.70; H, 2.39; N, 7.61. Elemental Anal. Calcd (%) for [Cr(phen)₂(bipy)](BF₄)₃·1.3H₂O: C, 47.91; H, 3.15; N, 9.86. Found: C, 47.87; H, 3.16; N, 9.83.

Preparation of [Cr(phen)₂(dpma)](CF₃SO₃)₃ (10). The complex was synthesized according to the general synthetic method described for [Cr(phen)₂(N–N')](CF₃SO₃)₃ complexes.

[Cr(phen)₂Cl₂]Cl (200 mg, 0.387 mmol, 1 equiv), trifluoromethanesulfonic acid (2 mL), di(pyrid-2-yl)(methyl)amine (143 mg, 0.772 mmol, 2 equiv), and 2,6-lutidine (90 μL, 0.772 mmol, 2 equiv) were reacted with a reaction time of 2 h. This method afforded pure [Cr(phen)₂(dpma)](CF₃SO₃)₃ (241 mg, yield 60%). Slow diffusion of Et₂O into a solution of [Cr(phen)₂(dpma)](CF₃SO₃)₃ in methanol provided single crystals suitable for XRD. ESI-MS *m/z*: [[Cr(phen)₂(dpma)](CF₃SO₃)₂]⁺, 895.3. Elemental Anal. Calcd (%) for [Cr(phen)₂(dpma)](CF₃SO₃)₃·0.35H₂O: C, 43.42; H, 2.66; N, 9.33. Found: C, 43.31; H, 2.55; N, 9.25.

Photophysical Measurements. Absorption spectra in solution were recorded using a Lambda 1050 PerkinElmer spectrometer (quartz cell path length 1 cm or 1 mm, 300–800 nm domain). Absorption spectra in the solid state were recorded on a Lambda 900 PerkinElmer spectrometer equipped with an integration sphere (background recorded on MgO). Emission spectra (excitation at 355 nm) and excitation spectra were recorded for frozen solution samples (acetonitrile/propionitrile 6/4 at *C* ≈ 5 × 10^{−3} mol L^{−1}), for powder samples at 10 K or for freeze–pump–thaw degassed acetonitrile solution (*C* ≈ 10^{−4} mol L^{−1}) at 293 K, with a Fluorolog (Horiba Jobin-Yvon) instrument, equipped with iHR320, a xenon lamp 450 W illuminator (FL-1039A/40A), and a water-cooled photomultiplier tube (PMT Hamamatsu R2658 or R928). The spectra were corrected for the spectral response of the system. For time-resolved experiments, the decay curves were collected on solution samples (acetonitrile/propionitrile 6/4 at *C* ≈ 5 × 10^{−3} mol L^{−1}) within the 10–300 K range, with a photomultiplier (Hamamatsu R2658 or R928) and a digital oscilloscope (Tektronix MDO4104C). Pulsed excitation at 355 nm was obtained with the third harmonic of a pulsed Nd:YAG laser (Quantel Qsmart850). Low temperatures were achieved with a closed-cycle cryosystem (Janis, CCS-900/204N) with the sample sitting in exchange gas (helium) for efficient cooling. Microcrystalline samples or acetonitrile/propionitrile (6/4) solutions (*C* ≈ 5 × 10^{−3} mol L^{−1}) were mounted in a glass capillary (1.2 mm interior diameter, glass cutoff at 320 nm) and stuck on copper plates with Agar Scientific silver paint (G3691). The copper plates were attached to the sample holder with silver paint as well. The oxygen free decay curve measurements were done at 293 K on acetonitrile solutions of the complex (*C* ≈ 10^{−4} mol L^{−1}). The complexes in a quartz tube were dissolved in acetonitrile and then degassed by freeze–pump–thaw, and filled with argon.

X-ray Crystallography. All data were collected on a Rigaku Supernova diffractometer equipped with a CCD ATLAS detector using Mo or Cu Kα radiation. The crystals were mounted on Mitegen cryoloops and held at 180 K in the cold stream of a cryostream (Oxford Cryosystems). Structures were solved using the dual-space algorithm implemented in SHELXT,⁸⁵ or using direct methods within the SIR2004 program.⁸⁶ They were refined using the full-matrix least-squares method on *F*² in the SHELXL program,⁸⁷ within the framework of Olex2 software.⁸⁸

■ ASSOCIATED CONTENT

§ Supporting Information

The Supporting Information is available free of charge on the ACS Publications website at DOI: 10.1021/acs.inorgchem.8b02530.

Crystallographic data; absorption, excitation, and emission spectrum; list of transition bands; list of lifetimes; and decay curves (PDF)

Accession Codes

CCDC 1865017–1865025 contain the supplementary crystallographic data for this paper. These data can be obtained free of charge via www.ccdc.cam.ac.uk/data_request/cif, or by emailing data_request@ccdc.cam.ac.uk, or by contacting The

Cambridge Crystallographic Data Centre, 12 Union Road, Cambridge CB2 1EZ, UK; fax: +44 1223 336033.

AUTHOR INFORMATION

Corresponding Authors

*E-mail: benjamin.doistau@unige.ch.

*E-mail: claude.piguet@unige.ch.

ORCID

Benjamin Doistau: 0000-0002-4767-1149

Céline Besnard: 0000-0001-5699-9675

Present Address

[§]G.C.: Centre de Biophysique Moléculaire (CBM); UPR CNRS 4301, Rue Charles Sadron, F-45071 Orléans cedex 2, France.

Author Contributions

The manuscript was written through contributions of all authors. All authors have given approval to the final version of the manuscript.

Funding

Financial support from the Swiss National Science Foundation is gratefully acknowledged.

Notes

The authors declare no competing financial interest.

ACKNOWLEDGMENTS

K. L. Buchwalder is acknowledged for performing elemental analysis.

REFERENCES

- (1) Büldt, L. A.; Wenger, O. S. Chromium Complexes for Luminescence, Solar Cells, Photoredox Catalysis, Upconversion, and Phototriggered NO Release. *Chem. Sci.* **2017**, *8*, 7359–7367.
- (2) Büldt, L. A.; Wenger, O. S. Luminescent Complexes Made from Chelating Isocyanide Ligands and Earth-abundant Metals. *Dalton Trans.* **2017**, *46*, 15175–15175.
- (3) Kahn, O.; Briat, B. Exchange Interaction in Polynuclear Complexes. Part 1-Principles, Model and Application to the Binuclear Complexes of Chromium(III). *J. Chem. Soc., Faraday Trans. 2* **1976**, *72*, 268–281.
- (4) Carlin, R. L.; Burriel, R. Magnetic Susceptibility of $\text{Cs}_2\text{CrCl}_5 \cdot 4\text{H}_2\text{O}$: Interplay of Exchange and Crystal-field Effects. *Phys. Rev. B: Condens. Matter Mater. Phys.* **1983**, *27*, 3012–3017.
- (5) Timco, G. A.; McInnes, E. J. L.; Winpenny, R. E. P. Physical studies of Heterometallic Rings: An Ideal System for Studying Magnetically-coupled Systems. *Chem. Soc. Rev.* **2013**, *42*, 1796–1806.
- (6) Morsing, T. J.; Sauer, S. P. A.; Weihe, H.; Bendix, J.; Døssing, A. Magnetic Interactions in Oxide-bridged Dichromium(III) Complexes. Computational Determination of the Importance of Non-bridging Ligands. *Inorg. Chim. Acta* **2013**, *396*, 72–77.
- (7) Collison, D.; Murrie, M.; Oganessian, V. S.; Piligkos, S.; Poolton, N. R. J.; Rajaraman, G.; Smith, G. M.; Thomson, A. J.; Timko, G. A.; Wernsdorfer, W.; Winpenny, R. E. P.; McInnes, E. J. L. Magnetic and Optical Studies on an $S = 6$ Ground-State Cluster $[\text{Cr}_{12}\text{O}_9(\text{OH})_3(\text{O}_2\text{CCMe}_3)_{15}]$: Determination of, and the Relationship Between, Single-Ion and Cluster Spin Hamiltonian Parameters. *Inorg. Chem.* **2003**, *42*, S293–S303.
- (8) Novosel, N.; Žilić, D.; Pajić, D.; Jurić, M.; Perić, B.; Zadro, K.; Rakvin, B.; Planinić, P. EPR and Magnetization Studies on Single Crystals of a Heterometallic (Cu(II) and Cr(III)) Complex: Zero-field Splitting Determination. *Solid State Sci.* **2008**, *10*, 1387–1394.
- (9) Alonso, P. J.; Arauzo, A. B.; Garcia-Monforte, M. A.; Garcia-Rubio, I.; Martin, A.; Menjon, B.; Rillo, C. Synthesis, Characterisation and Magnetic Properties of Octahedral Chromium(III) Compounds with Six C-donor Ligands. *Dalton Trans.* **2011**, *40*, 853–861.

(10) Padhi, S. K.; Saha, D.; Sahu, R.; Subramanian, J.; Manivannan, V. Synthesis, Structure, Optical and Magnetic Properties of $[\text{Cr}(\text{L}(\text{X})_3)]$, $\{\text{L} = 4'-(2\text{-pyridyl})-2,2':6',2''\text{-terpyridine}; \text{X} = \text{Cl}^-, \text{N}_3^-, \text{NCS}^-\}$. *Polyhedron* **2008**, *27*, 1714–1720.

(11) Scarborough, C. C.; Lancaster, K. M.; DeBeer, S.; Weyhermüller, T.; Sproules, S.; Wieghardt, K. Experimental Fingerprints for Redox-Active Terpyridine in $[\text{Cr}(\text{tpy})_2](\text{PF}_6)_n$ ($n = 3-0$), and the Remarkable Electronic Structure of $[\text{Cr}(\text{tpy})_2]^{1+}$. *Inorg. Chem.* **2012**, *51*, 3718–3732.

(12) Mallah, T.; Thiébaud, S.; Verdager, M.; Veillet, P. High- T_C Molecular-Based Magnets: Ferrimagnetic Mixed-Valence Chromium-(III)-Chromium(II) Cyanides with T_C at 240 and 190 K. *Science* **1993**, *262*, 1554.

(13) Verdager, M.; Bleuzen, A.; Marvaud, V.; Vaissermann, J.; Seuleiman, M.; Desplanches, C.; Sculler, A.; Train, C.; Garde, R.; Gelly, G.; Lomench, C.; Rosenman, I.; Veillet, P.; Cartier, C.; Villain, F. Molecules to Build Solids: High T_C Molecule-based Magnets by Design and Recent Revival of Cyano Complexes Chemistry. *Coord. Chem. Rev.* **1999**, *190–192*, 1023–1047.

(14) McInnes, E. J. L.; Piligkos, S.; Timco, G. A.; Winpenny, R. E. P. Studies of Chromium Cages and Wheels. *Coord. Chem. Rev.* **2005**, *249*, 2577–2590.

(15) Marinescu, G.; Andruh, M.; Lloret, F.; Julve, M. Bis(oxalato)-chromium(III) complexes: Versatile Tectons in Designing Heterometallic Coordination Compounds. *Coord. Chem. Rev.* **2011**, *255*, 161–185.

(16) Sieber, R.; Decurtins, S.; Stoeckli-Evans, H.; Wilson, C.; Yufit, D.; Howard, J. A. K.; Capelli, S. C.; Hauser, A. A Thermal Spin Transition in $[\text{Co}(\text{bpy})_3][\text{LiCr}(\text{ox})_3]$ ($\text{ox} = \text{C}_2\text{O}_4^{2-}$; $\text{bpy} = 2,2'\text{-bipyridine}$). *Chem. - Eur. J.* **2000**, *6*, 361–368.

(17) Kou, H.-Z.; Zhou, B. C.; Gao, S.; Wang, R.-J. A 2D Cyano- and Oxamidato-Bridged Heterotrimetallic Cr(III)-Cu(II)-Gd(III) Complex. *Angew. Chem., Int. Ed.* **2003**, *42*, 3288–3291.

(18) Otto, S.; Grabolle, M.; Förster, C.; Kreitzer, C.; Resch-Genger, U.; Heinze, K. $[\text{Cr}(\text{ddpd})_2]^{3+}$: A Molecular, Water-Soluble, Highly NIR-Emissive Ruby Analogue. *Angew. Chem., Int. Ed.* **2015**, *54*, 11572–11576.

(19) Kandasamy, B.; Ramar, G.; Zhou, L.; Han, S.-T.; Venkatesh, S.; Cheng, S.-C.; Xu, Z.; Ko, C.-C.; Roy, V. A. L. Polypyridyl Chromium(III) Complexes for Non-volatile Memory Application: Impact of the Coordination Sphere on Memory Device Performance. *J. Mater. Chem. C* **2018**, *6*, 1445–1450.

(20) McDaniel, A. M.; Tseng, H.-W.; Damrauer, N. H.; Shores, M. P. Synthesis and Solution Phase Characterization of Strongly Photooxidizing Heteroleptic Cr(III) Tris-Dipyridyl Complexes. *Inorg. Chem.* **2010**, *49*, 7981–7991.

(21) Stevenson, S. M.; Shores, M. P.; Ferreira, E. M. Photooxidizing Chromium Catalysts for Promoting Radical Cation Cycloadditions. *Angew. Chem., Int. Ed.* **2015**, *54*, 6506–6510.

(22) Higgins, R. F.; Fatur, S. M.; Shepard, S. G.; Stevenson, S. M.; Boston, D. J.; Ferreira, E. M.; Damrauer, N. H.; Rappé, A. K.; Shores, M. P. Uncovering the Roles of Oxygen in Cr(III) Photoredox Catalysis. *J. Am. Chem. Soc.* **2016**, *138*, 5451–5464.

(23) Stevenson, S. M.; Higgins, R. F.; Shores, M. P.; Ferreira, E. M. Chromium Photocatalysis: Accessing Structural Complements to Diels-Alder Adducts with Electron-deficient Dienophiles. *Chem. Sci.* **2017**, *8*, 654–660.

(24) Maeda, K.; Teramura, K.; Lu, D.; Takata, T.; Saito, N.; Inoue, Y.; Domen, K. Photocatalyst Releasing Hydrogen from Water. *Nature* **2006**, *440*, 295.

(25) Kirk, A. D. Chromium(III) Photochemistry and Photophysics. *Coord. Chem. Rev.* **1981**, *39*, 225–263.

(26) Jamieson, M. A.; Serpone, N.; Hoffman, M. Z. Advances in the Photochemistry and Photophysics of Chromium(III) Polypyridyl Complexes in Fluid Media. *Coord. Chem. Rev.* **1981**, *39*, 121–179.

(27) Forster, L. S. The Photophysics of Chromium(III) Complexes. *Chem. Rev.* **1990**, *90*, 331–353.

(28) Kirk, A. D. Photochemistry and Photophysics of Chromium-(III) Complexes. *Chem. Rev.* **1999**, *99*, 1607–1640.

- (29) Forster, L. S. Thermal Relaxation in Excited Electronic States of d^3 and d^6 Metal Complexes. *Coord. Chem. Rev.* **2002**, *227*, 59–92.
- (30) Ryu, C. K.; Endicott, J. F. Synthesis, Spectroscopy, and Photophysical Behavior of Mixed-ligand Mono- and Bis(polypyridyl)-chromium(III) Complexes. Examples of Efficient, Thermally Activated Excited-state Relaxation without Back Intersystem Crossing. *Inorg. Chem.* **1988**, *27*, 2203–2214.
- (31) Zare, D.; Doistau, B.; Nozary, H.; Besnard, C.; Guenee, L.; Suffren, Y.; Pele, A.-L.; Hauser, A.; Piguet, C. Cr(III) as an Alternative to Ru(II) in Metallo-Supramolecular Chemistry. *Dalton Trans.* **2017**, *46*, 8992–9009.
- (32) Otto, S.; Dorn, M.; Förster, C.; Bauer, M.; Seitz, M.; Heinze, K. Understanding and Exploiting Long-lived Near-infrared Emission of a Molecular Ruby. *Coord. Chem. Rev.* **2018**, *359*, 102–111.
- (33) Aboshyan-Sorgho, L.; Besnard, C.; Pattison, P.; Kittilstved, K. R.; Aebischer, A.; Bünzli, J.-C. G.; Hauser, A.; Piguet, C. Near-Infrared→Visible Light Upconversion in a Molecular Trinuclear d–f–d Complex. *Angew. Chem., Int. Ed.* **2011**, *50*, 4108–4112.
- (34) Suffren, Y.; Zare, D.; Eliseeva, S. V.; Guénée, L.; Nozary, H.; Lathion, T.; Aboshyan-Sorgho, L.; Petoud, S.; Hauser, A.; Piguet, C. Near-Infrared to Visible Light-Upconversion in Molecules: From Dream to Reality. *J. Phys. Chem. C* **2013**, *117*, 26957–26963.
- (35) Zare, D.; Suffren, Y.; Guenee, L.; Eliseeva, S. V.; Nozary, H.; Aboshyan-Sorgho, L.; Petoud, S.; Hauser, A.; Piguet, C. Smaller than a Nanoparticle with the Design of Discrete Polynuclear Molecular Complexes Displaying Near-infrared to Visible Upconversion. *Dalton Trans.* **2015**, *44*, 2529–2540.
- (36) Suffren, Y.; Goleosorkhi, B.; Zare, D.; Guénée, L.; Nozary, H.; Eliseeva, S. V.; Petoud, S.; Hauser, A.; Piguet, C. Taming Lanthanide-Centered Upconversion at the Molecular Level. *Inorg. Chem.* **2016**, *55*, 9964–9972.
- (37) Charbonnière, L. J.; Hildebrandt, N. Lanthanide Complexes and Quantum Dots: A Bright Wedding for Resonance Energy Transfer. *Eur. J. Inorg. Chem.* **2008**, *2008*, 3241–3251.
- (38) Tanner, P. A.; Zhou, L.; Duan, C.; Wong, K.-L. Misconceptions in Electronic Energy Transfer: Bridging the Gap Between Chemistry and Physics. *Chem. Soc. Rev.* **2018**, *47*, 5234–5265.
- (39) Serpone, N.; Jamieson, M. A.; Henry, M. S.; Hoffman, M. Z.; Bolletta, F.; Maestri, M. Excited-state Behavior of Polypyridyl Complexes of Chromium(III). *J. Am. Chem. Soc.* **1979**, *101*, 2907–2916.
- (40) Kirk, A. D.; Porter, G. B. Luminescence of Chromium(III) Complexes. *J. Phys. Chem.* **1980**, *84*, 887–891.
- (41) Endicott, J. F.; Lessard, R. B.; Lynch, D.; Perkovic, M. W.; Ryu, C. K. Stereochemical and Electronic Contributions to 2E Chromium(III) Excited State Relaxation Behavior at 77K. *Coord. Chem. Rev.* **1990**, *97*, 65–79.
- (42) Barker, K. D.; Barnett, K. A.; Connell, S. M.; Glaeser, J. W.; Wallace, A. J.; Wildsmith, J.; Herbert, B. J.; Wheeler, J. F.; Kane-Maguire, N. A. P. Synthesis and Characterization of Heteroleptic $[\text{Cr}(\text{diimine})_3]^{3+}$ Complexes. *Inorg. Chim. Acta* **2001**, *316*, 41–49.
- (43) Donnay, E. G.; Schaeper, J. P.; Brooksbank, R. D.; Fox, J. L.; Potts, R. G.; Davidson, R. M.; Wheeler, J. F.; Kane-Maguire, N. A. P. Synthesis and Characterization of Tris(heteroleptic) Diimine Complexes of Chromium(III). *Inorg. Chim. Acta* **2007**, *360*, 3272–3280.
- (44) Isaacs, M.; Sykes, A. G.; Ronco, S. Synthesis, Characterization and Photophysical Properties of Mixed Ligand Tris(polypyridyl)-chromium(III) Complexes, $[\text{Cr}(\text{phen})_2\text{L}]^{3+}$. *Inorg. Chim. Acta* **2006**, *359*, 3847–3854.
- (45) Barbour, J. C.; Kim, A. J. I.; deVries, E.; Shaner, S. E.; Lovaasen, B. M. Chromium(III) Bis-Arylterpyridyl Complexes with Enhanced Visible Absorption via Incorporation of Intraligand Charge-Transfer Transitions. *Inorg. Chem.* **2017**, *56*, 8212–8222.
- (46) Constable, E. C.; Housecroft, C. E.; Neuburger, M.; Schonle, J.; Zampese, J. A. The Surprising Lability of Bis(2,2':6',2''-terpyridine)-chromium(III) Complexes. *Dalton Trans.* **2014**, *43*, 7227–7235.
- (47) Schönle, J.; Constable, E. C.; Housecroft, C. E.; Prescimone, A.; Zampese, J. A. Homoleptic and Heteroleptic Complexes of Chromium(III) Containing 4'-Diphenylamino-2,2':6',2''-Terpyridine Ligands. *Polyhedron* **2015**, *89*, 182–188.
- (48) Cantuel, M.; Bernardinelli, G.; Imbert, D.; Bünzli, J.-C. G.; Hopfgartner, G.; Piguet, C. A Kinetically Inert and Optically Active Cr(III) Partner in Thermodynamically Self-assembled Heterodimetallic Non-covalent d-f Podates. *J. Chem. Soc., Dalton Trans.* **2002**, 1929–1940.
- (49) Cantuel, M.; Bernardinelli, G.; Muller, G.; Riehl, J. P.; Piguet, C. The First Enantiomerically Pure Helical Noncovalent Tripod for Assembling Nine-Coordinate Lanthanide(III) Podates. *Inorg. Chem.* **2004**, *43*, 1840–1849.
- (50) Cantuel, M.; Gumy, F.; Bünzli, J.-C. G.; Piguet, C. Encapsulation of Labile Trivalent Lanthanides into a Homobimetallic Chromium(III)-containing Triple-stranded Helicate. Synthesis, Characterization, and Divergent Intramolecular Energy Transfers. *Dalton Trans.* **2006**, 2647–2660.
- (51) Aboshyan-Sorgho, L.; Cantuel, M.; Petoud, S.; Hauser, A.; Piguet, C. Optical Sensitization and Upconversion in Discrete Polynuclear Chromium–lanthanide Complexes. *Coord. Chem. Rev.* **2012**, *256*, 1644–1663.
- (52) Imbert, D.; Cantuel, M.; Bünzli, J.-C. G.; Bernardinelli, G.; Piguet, C. Extending Lifetimes of Lanthanide-Based Near-Infrared Emitters (Nd, Yb) in the Millisecond Range through Cr(III) Sensitization in Discrete Bimetallic Edifices. *J. Am. Chem. Soc.* **2003**, *125*, 15698–15699.
- (53) Vasudevan, S.; Smith, J. A.; Wojdyla, M.; McCabe, T.; Fletcher, N. C.; Quinn, S. J.; Kelly, J. M. Substituted Dipyrrophenazine Complexes of Cr(III): Synthesis, Enantiomeric Resolution and Binding Interactions with Calf Thymus DNA. *Dalton Trans.* **2010**, *39*, 3990–3998.
- (54) Gao, X. The crystal structure of $[\text{Cr}(\text{phen})_2\text{Cl}_2]\text{Cl}$ was previously reported with a different space group and unit cell. *cis-Dichloridobis(1,10-phenanthroline)chromium(III) Chloride*. *Acta Crystallogr., Sect. E: Struct. Rep. Online* **2011**, *67*, m139–m139.
- (55) Luck, R. L.; Gawryszewska, P.; Riehl, J. P. The crystal structure of $[\text{Cr}(\text{phen})_3](\text{ClO}_4)$ was reported by Tris(1,10-phenanthroline- N,N')chromium(III) Triperchlorate Hydrate. *Acta Crystallogr., Sect. C: Cryst. Struct. Commun.* **2000**, *56*, e238–e239.
- (56) Scarborough, C. C.; Sproules, S.; Doonan, C. J.; Hagen, K. S.; Weyhermüller, T.; Wieghardt, K. Scrutinizing Low-Spin Cr(II) Complexes. *Inorg. Chem.* **2012**, *51*, 6969–6982.
- (57) Pearson, R. G.; Munson, R. A.; Basolo, F. Mechanism of Substitution Reactions of Complex Ions. XV: Acid and Base Hydrolysis of Cis- and Trans-dichloro-bis-(ethylene-diamine)-chromium(III) Ion. *J. Am. Chem. Soc.* **1958**, *80*, 504–504.
- (58) Wang, C.; Otto, S.; Dorn, M.; Kreidt, E.; Lebon, J.; Sršan, L.; Di Martino-Fumo, P.; Gerhards, M.; Resch-Genger, U.; Seitz, M.; Heinze, K. Deuterated Molecular Ruby with Record Luminescence Quantum Yield. *Angew. Chem., Int. Ed.* **2018**, *57*, 1112–1116.
- (59) Breivogel, A.; Meister, M.; Förster, C.; Laquai, F.; Heinze, K. Excited State Tuning of Bis(tridentate) Ruthenium(II) Polypyridine Chromophores by Push–Pull Effects and Bite Angle Optimization: A Comprehensive Experimental and Theoretical Study. *Chem. - Eur. J.* **2013**, *19*, 13745–13760.
- (60) Jorgensen, C. K. Spectroscopy of Transition-group Complexes. *Adv. Chem. Phys.* **2007**, *5*, 33–146.
- (61) Lever, A. B. P. *Inorganic Electronic Spectroscopy*; Elsevier ed., 1984; p 126.
- (62) Kane-Maguire, N. A. P. Photochemistry and Photophysics of Coordination Compounds: Chromium. *Top. Curr. Chem.* **2007**, *280*, 37–67.
- (63) Perkovic, M. W.; Heeg, M. J.; Endicott, J. F. Stereochemical Perturbations of the Relaxation Behavior of (2E)Chromium(III). Ground-state X-ray Crystal Structure, Photophysics, and Molecular Mechanics Simulations of the Quasi-cage Complex $[\text{4,4',4''-Ethylidynetris(3-azabutan-1-amine)}]\text{chromium Tribromide}$. *Inorg. Chem.* **1991**, *30*, 3140–3147.

- (64) Hauser, A.; Maeder, M.; Robinson, W. T.; Murugesan, R.; Ferguson, J. Electronic and Molecular Structure of Tris(2,2'-bipyridine)chromium(3+). *Inorg. Chem.* **1987**, *26*, 1331–1338.
- (65) Lee, K.-W.; Hoggard, P. E. The Molecular Structure of Bipyridinium tris(bipyridine)chromium(III) Perchlorate. *Polyhedron* **1989**, *8*, 1557–1560.
- (66) Ohno, T.; Kato, S.; Kaizaki, S.; Hanazaki, I. Singlet-triplet transitions of aromatic compounds coordinating to a paramagnetic chromium(III) ion. *Inorg. Chem.* **1986**, *25*, 3853–3858.
- (67) König, E.; Herzog, S. Electronic spectra of tris(2,2'-bipyridyl) complexes—I: The chromium series $[\text{Cr}(\text{bipy})_3]z$, $z = +3, +2, +1, 0$. *J. Inorg. Nucl. Chem.* **1970**, *32*, 585–599.
- (68) Otto, S.; Scholz, N.; Behnke, T.; Resch-Genger, U.; Heinze, K. Thermo-Chromium: A Contactless Optical Molecular Thermometer. *Chem. - Eur. J.* **2017**, *23*, 12131–12135.
- (69) Morse, P. M. Diatomic Molecules According to the Wave Mechanics. II. Vibrational Levels. *Phys. Rev.* **1929**, *34*, 57–64.
- (70) Hansch, C.; Leo, A.; Taft, R. W. A Survey of Hammett Substituent Constants and Resonance and Field Parameters. *Chem. Rev.* **1991**, *91*, 165–195.
- (71) Kuehn, K.; Wasgestian, F.; Kupka, H. The Role of Hydrogen Vibrations in the Radiationless Deactivation of Chromium(III)-Alkylamine Complexes in their Lowest Doublet State. *J. Phys. Chem.* **1981**, *85*, 665–670.
- (72) Brown, N. K.; Geue, J. R.; Sargeson, M. A.; Moran, G.; Ralph, F. S.; Riesen, H. A Long-Lived ^2E State for a $\text{Cr}(\text{III})\text{N}_6$ Amine cChromophore at 298 K: $[\text{Cr}(\text{fac-Me}_5\text{-D}_{3\text{h}}\text{tricosaneN}_6)]\text{Cl}_3$. *Chem. Commun.* **1998**, 2291–2292.
- (73) Otto, S.; Förster, C.; Wang, C.; Resch-Genger, U.; Heinze, K. A Strongly Luminescent Chromium(III) Complex Acid. *Chem. - Eur. J.* **2018**, *24*, 12555–12563.
- (74) Einstein, A. Zur Quantentheorie der Strahlung. *Phys. Z.* **1917**, *18*, 121–128.
- (75) Strickler, S. J.; Berg, R. A. Relationship Between Absorption Intensity and Fluorescence Lifetime of Molecules. *J. Chem. Phys.* **1962**, *37*, 814–822.
- (76) Birks, J. B.; Dyson, D. J. The Relations Between the Fluorescence and Absorption Properties of Organic Molecules. *Proc. R. Soc. London, Ser. A* **1963**, *275*, 135–148.
- (77) Perkovic, M. W.; Endicott, J. F. Stereochemical Tuning of Chromium(III) Photophysics with N,N',N'' -Tris(alkylamine)-1,4,7- t -Triazacyclononane Complexes. *J. Phys. Chem.* **1990**, *94*, 1217–1219.
- (78) Fucaloro, A. F.; Forster, L. S.; Rund, J. V.; Lin, S. H. ^2E Relaxation in Mixed-Ligand $\text{Cr}(\text{NH}_3)_{6-n}\text{X}_n$ Complexes. *J. Phys. Chem.* **1983**, *87*, 1796–1799.
- (79) Rojas, G. E.; Magde, D. Temperature dependence of the doublet lifetime in chromium(III) compounds. *Inorg. Chem.* **1987**, *26*, 2334–2337.
- (80) Castelli, F.; Forster, L. S. Nonexponential Luminescence Decay in Hexaureachromium(III). *J. Am. Chem. Soc.* **1975**, *97*, 6306–6309.
- (81) Ji, S.; Guo, H.; Yuan, X.; Li, X.; Ding, H.; Gao, P.; Zhao, C.; Wu, W.; Wu, W.; Zhao, J. A Highly Selective OFF-ON Red-Emitting Phosphorescent Thiol Probe with Large Stokes Shift and Long Luminescent Lifetime. *Org. Lett.* **2010**, *12*, 2876–2879.
- (82) Wu, S. H.; Shao, J. Y.; Dai, X.; Cui, X.; Su, H.; Zhong, Y. W. Synthesis and Characterization of Tris(bidentate) Ruthenium Complexes of Di(pyrid-2-yl)(methyl)amine. *Eur. J. Inorg. Chem.* **2017**, *2017*, 3064–3071.
- (83) Hissler, M.; Connick, W. B.; Geiger, D. K.; McGarrah, J. E.; Lipa, D.; Lachicotte, R. J.; Eisenberg, R. Platinum Diimine Bis(acetylide) Complexes: Synthesis, Characterization, and Luminescence Properties. *Inorg. Chem.* **2000**, *39*, 447–457.
- (84) Burstall, F. H.; Nyholm, R. S. 681. Studies in Co-ordination Chemistry. Part XIII. Magnetic Moments and Bond Types of Transition-Metal Complexes. *J. Chem. Soc.* **1952**, 3570–3579.
- (85) Sheldrick, G. SHELXT - Integrated Space-group and Crystal-structure Determination. *Acta Crystallogr., Sect. A: Found. Adv.* **2015**, *71*, 3–8.
- (86) Burla, M. C.; Caliandro, R.; Camalli, M.; Carrozzini, B.; Cascarano, G. L.; De Caro, L.; Giacovazzo, C.; Polidori, G.; Spagna, R. SIR2004: an improved tool for crystal structure determination and refinement. *J. Appl. Crystallogr.* **2005**, *38*, 381–388.
- (87) Sheldrick, G. M. Crystal structure refinement with SHELXL. *Acta Crystallogr., Sect. C: Struct. Chem.* **2015**, *71*, 3–8.
- (88) Dolomanov, O. V.; Bourhis, L. J.; Gildea, R. J.; Howard, J. A. K.; Puschmann, H. OLEX2: a complete structure solution, refinement and analysis program. *J. Appl. Crystallogr.* **2009**, *42*, 339–341.